Surface Acoustic Wave Microfluidics

Leslie Y. Yeo and James R. Friend

MicroNanophysics Research Laboratory, RMIT University, and the Melbourne Centre for Nanofabrication, Melbourne, VIC 3001 Australia; email: leslie.yeo@rmit.edu.au, james.friend@rmit.edu.au

Annu. Rev. Fluid Mech. 2014. 46:379–406

First published online as a Review in Advance on September 20, 2013

The *Annual Review of Fluid Mechanics* is online at fluid.annualreviews.org

This article's doi:
10.1146/annurev-fluid-010313-141418

Keywords

ultrasonics, acoustics, lab on a chip, fluid-structural interaction, piezoelectrics, interfacial phenomena

Abstract

Fluid manipulations at the microscale and beyond are powerfully enabled through the use of 10–1,000-MHz acoustic waves. A superior alternative in many cases to other microfluidic actuation techniques, such high-frequency acoustics is almost universally produced by surface acoustic wave devices that employ electromechanical transduction in wafer-scale or thin-film piezoelectric media to generate the kinetic energy needed to transport and manipulate fluids placed in adjacent microfluidic structures. These waves are responsible for a diverse range of complex fluid transport phenomena—from interfacial fluid vibration and drop and confined fluid transport to jetting and atomization—underlying a flourishing research literature spanning fundamental fluid physics to chip-scale engineering applications. We highlight some of this literature to provide the reader with a historical basis, routes for more detailed study, and an impression of the field's future directions.

1. INTRODUCTION

Piezoelectric: material possessing a spontaneous electrical polarization in the unit cell of a crystal or grain of a polycrystalline material

Acoustic waves are easily generated within a piezoelectric material through the transduction of electric fields; such waves propagate within and onward to the boundaries of the material in diverse ways dependent on the field and material geometries. The incredible variety of wave types studied reveals the long history of the subject, and substantial progress has been made. Indeed, surface acoustic waves (SAWs) are a relatively recent development, the beneficiary of exhaustive research due to their usefulness to the telecommunications industry since the mid-1960s (Campbell 1998). SAWs may be formed along an interface when the material properties of one medium differ substantially from the other, under certain conditions imposed on the more rigid material. However, for the purposes of this review, the SAW is usually formed on a piezoelectric solid medium, a method made ubiquitous with the development of easily fabricated electrodes (White & Voltmer 1965). The most important aspect of SAWs is their relatively slow speed compared to the bulk wave speed of sound in the medium itself, causing the wave and its energy to be trapped on the surface (Friend & Yeo 2011), within a very few wavelengths.

One of the most attractive aspects of using SAWs for microfluidic actuation and manipulation is their very efficient fluid-structural coupling owing to the presence of most of the energy adjacent to the interface. The elastic energy present at high frequencies due to the SAW is responsible for extreme accelerations; at the maximum vibration velocity of order 1 m/s (see the sidebar Extreme Accelerations in High-Frequency Ultrasound), the acceleration is at least 10^8 m/s^2. This enables a host of microfluidic operations to be carried out entirely on a chip-scale substrate powered by a palm-sized portable electronic driver circuit (**Figure 1**) (Yeo & Friend 2009). By circumventing the need for large and cumbersome benchtop pumps or external power supplies such as amplifiers, signal generators, and transformers, SAW microfluidics therefore addresses one of the most fundamental constraints in microfluidics that precludes the widespread implementation of practical lab-on-a-chip devices: the delivery of a complete microfluidics solution at the microscale, including sample preparation and analyte detection (Yeo et al. 2010a). In what follows, we examine the different SAW microscale fluid actuation mechanisms developed to date and their use in various microfluidic applications, which span biomolecular and cellular manipulation and detection, drug delivery, biomaterials synthesis, and point-of-care diagnostics. The use of SAWs in sensing applications is both vast and beyond the scope of this review, so we only briefly discuss the use of SAW microfluidics for detection enhancement. The reader is instead referred to, for example, Fu et al. (2010), Hossenlopp (2006), Jakubik (2011), Länge et al. (2008), and references therein.

EXTREME ACCELERATIONS IN HIGH-FREQUENCY ULTRASOUND

The generation of acoustic waves with piezoelectric materials generally follows a curious rule of thumb: The maximum vibration velocity that may be induced in any such device, continuously, is of the order of 1 m/s regardless of the scale of the device or the frequency chosen. Consequently, it is reasonable to wonder why one would choose a SAW if one could use lower frequencies, such as audible frequencies (Oberti et al. 2009). Beyond the benefit of acoustic wavelengths in the fluid from SAW that correspond to the typical 1–100-μm dimensions of a microfluidics device, there is the advantage of extreme accelerations. The acceleration induced is a product of the frequency and the vibration velocity, and on reaching 10 MHz, for example, the acceleration induced is over 10^7 m/s^2, larger than any other known technique except for particle accelerators or synchrotrons (McMillan 1945). For this reason, it is possible to obtain extraordinary inertial behavior from fluids and particles down to the nanoscale, such as the ejection of nanoparticles from the surface of a SAW device (Tan et al. 2007a).

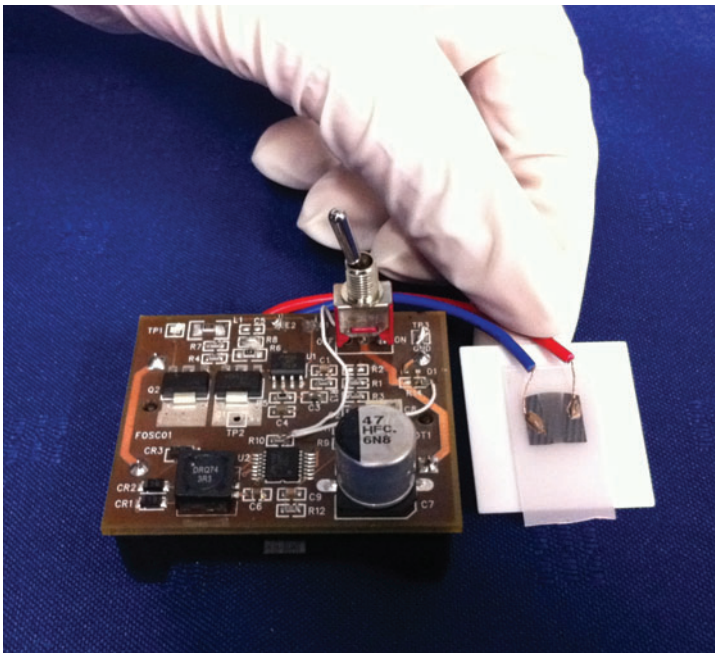

Figure 1

A prototype portable circuit on the left for driving the surface acoustic wave device on the right.

2. VIBRATION

Since the discoveries of Chladni (1787), Faraday (1831), and Kundt (1866), surface and bulk fluid vibrations have long constituted mechanisms by which particles can be concentrated or aligned at nodal or antinodal points along a standing wave, either imposed on the free surface of a vibrated liquid body in the former or induced as a pressure field in the bulk of the fluid as a consequence of reflections at the boundaries of the fluid body in the latter. The positioning of the nodes and (antinodes) can be altered by the presence of capillary waves or by a purposeful change of the boundary conditions (Tan et al. 2010a). Whether the particles assemble at nodes or antinodes is complicated by factors such as their size, density relative to the fluid, compressibility, and wettability (in the case of free surface vibrations), as discussed in Friend & Yeo (2011). Furthermore, the capillary waves themselves may exhibit a broadband, turbulent response that is difficult to predict; fascinating from a physical standpoint; and effective at driving the entire fluid sample into chaotic behavior, which eliminates the ability to effectively form regular patterns of particles within (Blamey et al. 2013). Nevertheless, the possibility of rapidly and precisely altering the positions at which the particles collect by simply switching the applied frequency and hence wavelength, together with other more advanced techniques such as varying the distribution of the vibration via more complex device resonance architectures (Laurell et al. 2007), offers an attractive method for spatial (and even temporal) control of particles in a microfluidic system for various applications, such as flow cytometry and DNA, protein, and cell microarray templating.

Most literature on particle manipulation reports the use of standing surface acoustic waves (SSAWs), reminiscent of the particle patterning reported in Kundt's (1866) tubes and more fundamental work examining the forces on a particle in a fluid (Doinikov 1996a,b, 2001; Gor'kov 1961). This also builds on the vast and similar body of work on ultrasonic standing waves, or what

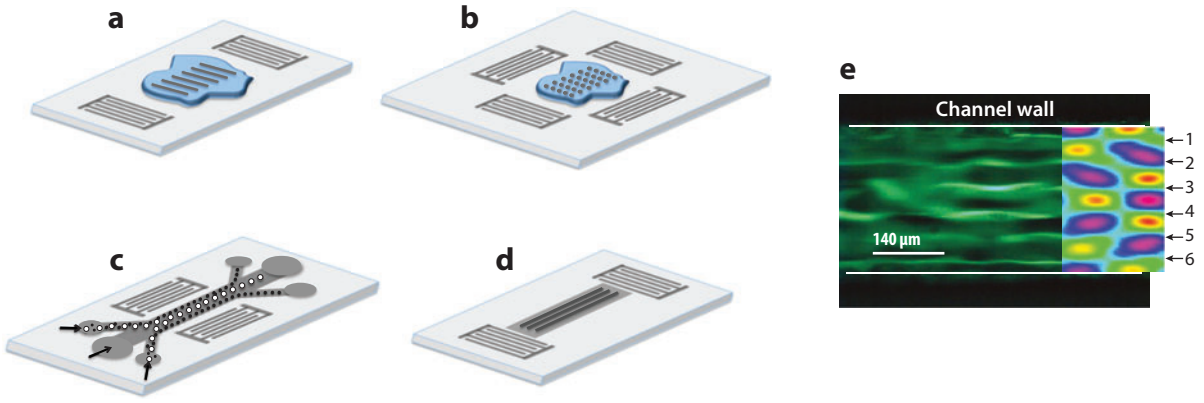

Figure 2

Schematic depiction of the various surface acoustic wave (SAW) particle alignment/focusing concepts (not to scale). (*a*) Transverse linear particle assemblies in a drop with a longitudinal standing surface acoustic wave (SSAW). In certain cases, the particle lines may appear to be curved similar to beaching curves (Li et al. 2008, Tan et al. 2007b) owing to SAW diffraction arising from the curvature of the drop contact line, as seen in **Figure 3*b***. A glass cover slide is occasionally mounted over the drop, providing stronger reflections and hence a standing sound wave in the bulk of the fluid (Wood et al. 2008). (*b*) Pointwise particle array in a drop (or within a confined fluid layer) with transverse and longitudinal SSAWs (Wood et al. 2009). Again, the patterns may be distorted by the drop shape because of contact line diffraction. (*c*) Longitudinal particle alignment and focusing using a transverse SSAW combined with a continuous laminar sheath flow within a microchannel bonded onto the substrate for possible downstream particle separation (Shi et al. 2008, 2009b, 2011). (*d*) Linear particle assemblies along the length of a microchannel cut into the SAW substrate using a longitudinal traveling SAW (Tan et al. 2009a). Similar assemblies can also be achieved with bonded microchannels atop the substrate. (*e*) Linear particle assemblies shown in panel *d*, with the particles collecting at lateral pressure nodes in the fluid channel, illustrated by the corresponding computed pressure distribution (*inset*). The six computed pressure nodes align with the experimentally observed collection lines.

is known as bulk acoustic waves (BAWs) (e.g., Hertz 1995, Laurell et al. 2007, and references therein). Wood et al. (2008) generated an SSAW and hence a vertical standing pressure wave in a fluid using two counterpropagating SAWs from interdigital transducers (IDTs) at opposite ends of the drop containing the particle suspension that was confined under a glass cover slide. Particles were then observed to aggregate into transverse linear assemblies corresponding to the nodal lines of the pressure wave, which in turn coincided with the nodes of the SSAW (**Figure 2*a***), whose spacing could be easily adjusted by tuning the SAW frequency. Such alignment of particles on nodal positions generated by the SAW contrasts with earlier work by Smorodin et al. (2005), Seemann et al. (2006), and Kong et al. (2010) using SAWs to align single- and multiwalled carbon nanotubes and larger structures, primarily owing to the electric field arising from the piezoelectric effect of the SAW (typically 10^6–10^7 V/m). Although it is claimed that the nanotubes align lengthwise primarily along the SAW propagation direction as a consequence of the dipole field, aided by the streaming, it is not clear from Kong et al.'s (2010) work that the alignment does not, at least in part, result from dielectrophoretic effects (motion due to an induced dipole moment on a particle in the presence of a nonuniform electric field) (Pethig 2010). Although the dielectrophoretic forces are typically too weak to drive particle motion at nanometer scales, they are known to drive alignment of the nanotubes owing to the latter's enhanced conductivity (Chang & Yeo 2010). Indeed, Kong et al. (2010) demonstrated the role of the dielectrophoretic force in aligning micrometer-dimension rod-like metallic structures: When the electric field was screened, no alignment was observed.

Bulk acoustic wave (BAW): waves that propagate in the solid bulk, including a variety of distinct waves in solids (e.g., Love, Lamb, and flexural)

The SSAW linear particle assemblies in Wood et al. (2008) were later extended to produce an array of pointwise assemblies by generating another orthogonal SSAW using two additional

IDTs in the transverse *y*-crystal direction (**Figure 2*b***), exploiting the weak SAW present along the off-axis *y* direction and illustrating the low power requirements for this particular application (Wood et al. 2009). As with the particle line spacing, spatial control in the transverse direction has also been demonstrated through the adjustment of the *y*-axis propagating SAW frequency. In principle, however, only two orthogonally arranged IDTs, instead of the four in Wood et al. (2009), are required if solid boundaries confine the fluid. For example, Shi et al. (2009a) placed a square polydimethylsiloxane (PDMS; Friend & Yeo 2010) chamber atop the SAW substrate. This was an extension of their preceding work on particle focusing using two IDTs to set up an SSAW transverse to the continuous laminar flow along a long PDMS channel driven using capillary pumps (Shi et al. 2008) (**Figure 2*c***). The particle spacing along the channel can also be varied with the use of tapered interdigital transducers (tIDTs) to modify the SAW frequency and hence wavelength along the sides of the channel in the one-dimensional and two-dimensional configurations (Ding et al. 2012b). This also hints at the difficulties resulting from the presence of boundaries, where the acoustic impedance changes from one medium to the next: Even though PDMS and water have similar acoustic impedances, reflections from a PDMS/water interface are strong enough to cause standing waves. Chirped IDTs possess a variation in the finger periodicity (width and spacing) that has been used to achieve the same effect and for even finer manipulation (e.g., trapping, translation, and elongation) of single particles, cells, and organisms, although the individual particles or cells have to first be isolated as the SAW cannot as yet be employed to segregate a single entity from a cluster (Ding et al. 2012a).

Unlike particle alignment on dry vibrating substrates (see, e.g., Tan et al. 2007a), particles do not align directly on the displacement or pressure nodes (or antinodes) of the SSAW itself. This is widely misunderstood and improperly presented in the majority of the work on SSAW particle manipulation. In fact, particles align with and aggregate onto the pressure nodes of the standing sound wave within the fluid (i.e., the BAW). This is a consequence of the acoustic waves radiated into the fluid from the SSAW (i.e., leaky SAW) reflecting off the channel or chamber walls in both cases to produce standing waves in the fluid. There are strong reflections in unconfined fluids as well, both at the free surface of the fluid and at the solid-fluid interface, that give rise to a standing sound wave in the bulk of the drop before the propagating wave decays due to viscous dissipation (Johansson et al. 2012b, Tan et al. 2010a). At times, the BAW in the fluid is somewhat aligned with the SSAW; at other times, it most certainly is not (Tan et al. 2010a). In any case, one has to carefully choose the frequency such that the channel width accommodates only one pressure node and hence one line of focused particles—if a single line of aligned particles is desired. Strictly speaking, therefore, it is the sound wavelength in the fluid, and not the SAW wavelength, that should be considered together with the channel width (Tan et al. 2009a), although both are related and the particles should focus into a line along the centerline of the channel if the sound wave reflection off its walls is symmetric.

Subsequent work by the same group suggested the possibility for alignment and focusing of particles across the channel depth (Shi et al. 2011), although the principle appears to be based on standing sound waves being generated in the fluid. Conceivably, the same mechanism (i.e., the standing BAW in the fluid) is responsible for the particle alignment in both the two-dimensional and three-dimensional focusing experiments (and not the direct effect by the SSAW in the former). The focusing across the channel depth may have been difficult to observe in the former experiment, and we also note that the channel was twice as deep in the latter work. Further manipulation of the aligned particle assemblies can be achieved, for example, by varying the relative phase φ between the two input signals to the IDT, which results in a linear translation in the position of the pressure node (Meng et al. 2011); particles can be translated a distance $\Delta x = \varphi/2k$, where k is the wave number. This really only works if the reflection at the channel walls is weak, as the standing

wave across the channel defined by the width of the fluid channel will interfere with the ability to perform phase shift manipulation. Such phase shifting was employed to alter the positions of the particle alignment (Meng et al. 2011, Orloff et al. 2011), which is useful for the downstream separation of particle species (see below) and marching single cells and bubbles in one and two dimensions (Meng et al. 2011, 2012; O'Rorke et al. 2012). The ease of varying the phase using voltage control makes it particularly attractive in microfluidic systems for particle manipulation. More recently, Tran et al. (2012) demonstrated that a similar phase shift (albeit a dynamic relative phase shift in contrast to that above) between the generation and reflection IDTs can be generated through the application of a slight frequency modulation from the IDT resonance to induce the same SSAW particle manipulation in two dimensions. Particle species can be acoustophoretically separated (Durand Vidal et al. 2001, Lin et al. 2012) as they are aligned or focused by exploiting the difference in the forces experienced across different species.

Given that sedimentation forces are relatively small at these scales, the acoustic radiation pressure-driven forces and viscous drag dominate the particle motion. The acoustic radiation forces scale with a^3 for SSAWs and a^6 for traveling SAWs (Friend & Yeo 2011), and the viscous drag scales linearly with respect to the particle size a. Below a frequency-dependent critical crossover size (Rogers et al. 2010), the drag force dominates, whereas above this crossover, the acoustic force dominates. Shi et al. (2009b) made use of this size-dependent discrimination in the forces to separate two particle species of similar density but with different sizes in a continuous sheath flow, as larger species focus onto the pressure node at the center of the channel much faster than the smaller species above the crossover size. Guldiken et al. (2012) later demonstrated this in the absence of a sheath flow. Given the different particle trajectories along the channel length, the different species can therefore be separated through channel bifurcations downstream (the separation efficiency can be improved by adjusting the channel length, flow rate, or the SSAW frequency and power) (**Figure 2*c***). In addition to size separation, particles can also be separated based on density and compressibility—especially useful, for example, for sorting viable and nonviable biological entities or for removing debris and other sample contaminants—given the dependence of the acoustic force on the acoustic contrast factor, a ratio dependent on the density difference between the fluid and particles within the fluid (e.g., Raeymaekers et al. 2011, equation 6). Differences in the acoustic contrast factor were, for example, exploited by Nam et al. (2011) and Jo & Guldiken (2012). Nam et al. (2011), in particular, demonstrated the separation of platelets from whole blood and even the separation of particles encapsulated with cells of different number densities (Nam et al. 2012), with high separation efficiencies (>97%) but with very small throughputs (of the order of 0.1–10 μl/min and ∼2,000 particles/min) compared to the 10^3∼10^4 particles/s typical of the most efficient microfluidic sorters and conventional fluorescence-activated cell-sorting devices.

Another example of the use of SSAWs for dynamic patterning is the creation of transverse periodic lipid concentration localization in supported lipid bilayer membranes (Hennig et al. 2009). Alvarez et al. (2008a) had earlier shown such macromolecular patterning in which long-range regularly ordered polymer arrays, whose spot dimension and spacing strongly correlate with the SAW wavelength and hence applied frequency, were generated by a combination of traveling SAWs and SSAWs. The traveling wave component allowed a drop containing the polymer solution to be translated across the SAW substrate, leaving behind a trailing film. As a consequence of the longitudinal and transverse instabilities induced by the SAW acceleration at the film interface, the solvent rapidly atomized (Qi et al. 2008; see Section 5) to form a two-dimensional array of polymer spot residues on the substrate in a hexagonally close-packed arrangement (**Figure 3*a***), demonstrating the potential of the technique for fast substrate patterning without physical or chemical templating. Whereas other instances of traveling SAWs for particle manipulation have also been explored in the context of microchannel flows, we note that longitudinal

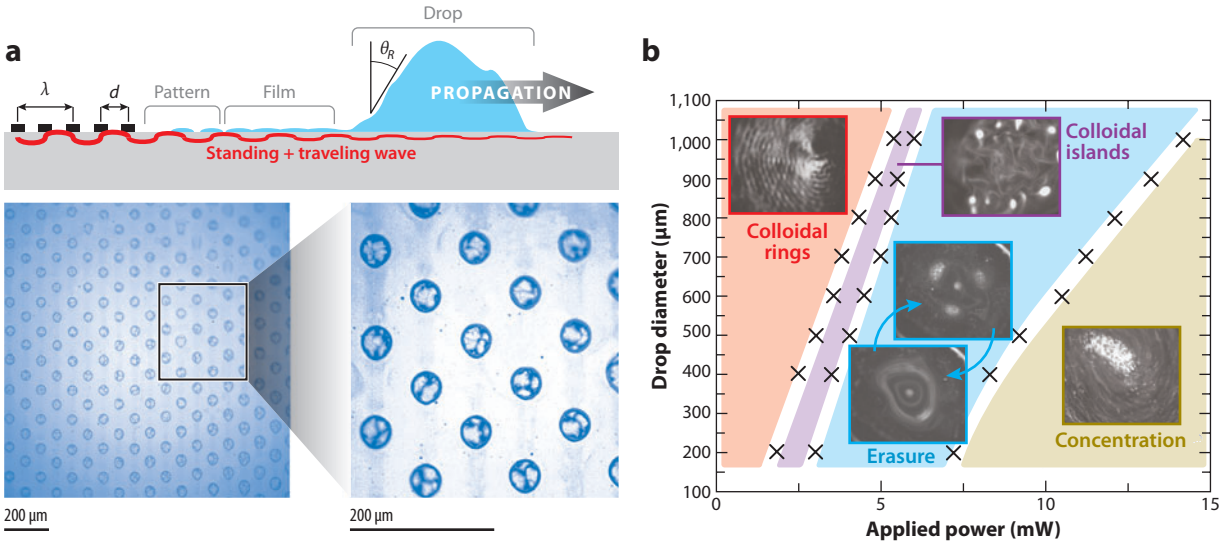

Figure 3

Other examples of vibration-induced patterning. (*a*) Long-range hexagonal close-packed ordering of polymer spot patterns generated through longitudinal and transverse interfacial instabilities of the atomizing film trailing a drop of polymer solution translated with traveling and standing surface acoustic waves (SAWs) (*schematic*). Panel *a* modified from Alvarez et al. (2008a). (*b*) Colloidal patterning on the free surface of a sessile drop induced by capillary wave vibration, illustrating the different patterns obtained as the power is increased for a drop of fixed dimension (moving horizontally from left to right). At low powers, linear colloidal assemblies are observed, whose spacing correlates with the SAW wavelength, similar to those shown in **Figure 2*a***. At higher powers when the entire drop undergoes a breathing mode vibration associated with a circular nodal ring, the intersection between the nodal lines associated with the SAW wavelength and the nodal ring gives rise to pointwise island assemblies. As the power is further increased, streaming in the drop causes these islands to be erased; however, this phenomenon appears to be cyclic. When the streaming ceases, the islands reform, only to be dispersed again when the streaming resumes. At the high-power extreme, strong constant streaming within the drop causes either the dispersion or concentration of the colloids (Li et al. 2007b, Shilton et al. 2008), discussed in Section 3. Panel *b* modified from Li et al. (2008).

particle alignment still occurs along pressure nodes of a standing wave transverse to a channel that results from the reflections of the sound wave in the fluid at the channel walls (**Figure 2*d*,*e***), the sound wave arising as a consequence of leaky SAWs in the fluid (Tan et al. 2009a). A fundamental difference between the traveling SAWs in Tan et al. (2009a) and SSAWs in Shi et al. (2009a,b) is the placement of the IDT and hence the direction of the SAW with respect to the channel. Despite the standing BAW in the fluid orthogonal to the channel along which the particles align in both cases, the SAW propagates longitudinally along the channel in the former and orthogonal to the channel in the latter. Although both cases therefore facilitate the same particle alignment and control within the channel, an advantage of using traveling SAWs is the ability to transport the fluid and hence transport the channels using the SAWs (Tan et al. 2009a), therefore circumventing the need for external capillary pumps; such SAW-driven microchannel fluid actuation is discussed in Section 3.2.

Besides linear particle aggregation, it is also possible to carry out more complex particle manipulation, for example, by exploiting other vibration modes or the intersection of a series of nodal lines. Li et al. (2008) showed that particles in the linear assemblies clustered into pointwise island assemblies arising from the intersection of the nodal lines associated with low-amplitude, high-frequency (i.e., the SAW frequency) capillary waves and the circular nodal ring associated

with large-amplitude capillary waves at the capillary-viscous resonant frequency of the drop (**Figure 3*b***). Each nodal intersection gave rise to a particle cluster that could be dynamically erased at higher applied powers when streaming in the drop ensued but that reformed when the streaming ceased. The number of nodal intersections and hence particle clusters clearly depended on the drop dimension but was seen to dynamically evolve as the drop dimension varied, for example, as it evaporated. Other alternatives for microfluidic particle manipulation are discussed in Section 3.3, including the use of direct acoustic forces on the particles and fluid flow to influence particle motion (e.g., the use of microcentrifugation to concentrate and separate particles).

3. ACTUATION

The inverse scaling of the capillary pressure and the quartic scaling of the volumetric flow rate, both with respect to the channel dimension, reveal the inherent difficulty of driving microscale fluid actuation in which viscous and surface forces dominate (Yeo et al. 2010a). This is compounded by the existence of disjoining pressure effects that complicate the wettability control of drops in open microfluidic platforms. Consequently, there are few efficient ways to move and manipulate fluids in microchannels. Fortunately, SAW offers a solid-state actuation mechanism, free from moving parts susceptible to wear and reliability constraints, offering an efficient and compact scheme appropriate for integration for drop transport, microchannel transport, and microcentrifugation.

3.1. Drop Translation

SAW drop transport and manipulation are enabled by the ability of the time-averaged body force exerted on the entire drop—a consequence of the bulk streaming that arises as acoustic energy is transmitted into the drop (Friend & Yeo 2011)—to overcome the pinning of the drop contact line (Beyssen et al. 2006, Brunet et al. 2010, Tan et al. 2007b). In the past decade, various groups have exploited this to translate drops on the SAW substrate at speeds of the order of centimeters per second (slightly higher with focused IDTs) (Ai & Marrone 2012). For example, SAWs were used to rapidly drive drops comprising a suspension of cells into scaffolds for three-dimensional cell culture in tissue or orthopedic engineering (Bok et al. 2009, Li et al. 2007a). Compared to capillary-gravity-assisted seeding, which is painfully slow and leads to most cells being seeded only along the scaffold periphery, cells driven into the scaffold using SAW-assisted drop translation were found to penetrate deeply, thereby facilitating a more uniform seeding density. In other work, SAWs were employed to dispense and transport individual drops (Renaudin et al. 2006) to different heater locations on an open polymerase chain reaction platform, in which it was claimed that the mixing in the drop due to the SAW streaming (Alghane et al. 2011; Shilton et al. 2008, 2011b) led to enhanced hybridization efficiencies (Wixforth et al. 2004). The drops' positions may be determined using an echo-localization method (Renaudin et al. 2009). However, more recently Travagliati et al. (2012) demonstrated the possibility of detecting the presence of a drop and positioning it. This led to the design of integrated logic gates without a feedback control requirement by incorporating two Bragg reflectors comprising parallel short-circuited periodic strips between the IDTs to form a cavity for the traveling SAW. A SAW that matches the resonance of the cavity is therefore fully transmitted in the absence of a fluid loading on the cavity pad but is nearly fully reflected when the drop is in (and trapped by) the cavity. Simultaneously, the SAW may be used to detect the presence of the drop, and the drop can then be routed to other locations and exploited for other sequential operations.

The rapid translation of sessile drops on open platforms can also be used for bioparticle collection, sampling, and concentration (Tan et al. 2007b) and for subsequent downstream

CLASSIC TERMS FOR ACOUSTIC STREAMING

Eckart streaming is acoustic streaming within the fluid bulk, away from the sound source (Eckart 1948). It appears over length scales greater than one sound wavelength in the fluid, due to viscous attenuation of the sound radiating into the fluid from the source. If the fluid size is less than one wavelength, this streaming may not appear.

Rayleigh streaming is acoustic streaming in the bulk of a fluid typically in a vortical pattern, with each vortex having a scale of one wavelength in the fluid (Rayleigh 1884). It appears because of streaming present in the viscous boundary layer surrounding the fluid bulk.

Schlichting streaming is acoustic streaming within the viscous boundary layer toward the source of acoustic energy due to viscous attenuation (Schlichting 1932). Because the viscous boundary layer is typically much smaller than the acoustic wavelength, this streaming is the most fine-grained of the three.

All these streaming terms are used in the literature as extensions of the forms of streaming reported by the respective authors, and not always correctly. The important aspects to keep in mind are the dominance of one form of streaming over another, depending on the scale of the fluid system, and the potential to have all three forms of streaming, giving rise to very complex phenomena.

detection, for example, in combination with surface plasmon resonance (Galopin et al. 2007). Careful heat management is crucial because heating due to the viscous absorption of the BAW in the fluid arising from SAW leakage has been reported to reduce the signal reflectance (Renaudin et al. 2010). Nevertheless, not only is the SAW useful here to enhance detection sensitivity through the convective transport of target analytes to the binding sites, but additionally the SAW streaming can be harnessed to hydrodynamically shear unbound or nonspecifically bound targets (Sankaranarayanan et al. 2008, 2010). In a similar manner, the shear stresses imposed by the SAW streaming have also been employed to stretch and unfold von Willebrand factor fibers—repeated protein dimer units that play a crucial role in mediating the blood-clotting process by regulating platelet adhesion to damaged blood vessel walls—beyond a critical shear rate that triggers a globule stretch transition (Schneider et al. 2008b).

3.2. Microchannel Transport

Cecchini et al. (2008) reported the first SAW microchannel transport mechanism, in which liquid was drawn through a PDMS microchannel placed atop the SAW substrate in the direction opposing SAW propagation (**Figure 4*a***). Rather than a typical pump mechanism, the reported flow is actually a result of atomization of the meniscus that deposits droplets ahead of the meniscus front, which subsequently coalesce with the front to cause it to advance as the authors claim, albeit very slowly. If the surface tension is reduced, a thin film can be drawn out from the fluid drop owing to Rayleigh streaming, which propagates at a higher speed toward the SAW source than with the atomization-driven front advancement (Rezk et al. 2012a) (see the sidebar Classic Terms for Acoustic Streaming). Upon reaching the IDT providing the source of acoustic radiation, it thickens until Eckart streaming takes over, forcing the rapid flow of rivulets of fluid in the direction of SAW propagation.

Microparticles placed into a system reminiscent of Cecchini et al. (2008) can be shown to collect in cross-channel patterns that illustrate how a leaky SAW decays in only a few wavelengths along the fluid channel from the IDT source (Manor et al. 2012). Liquid actuation in a two-dimensional 5 × 5 square microchannel grid was demonstrated using multiple IDTs arranged at the entry

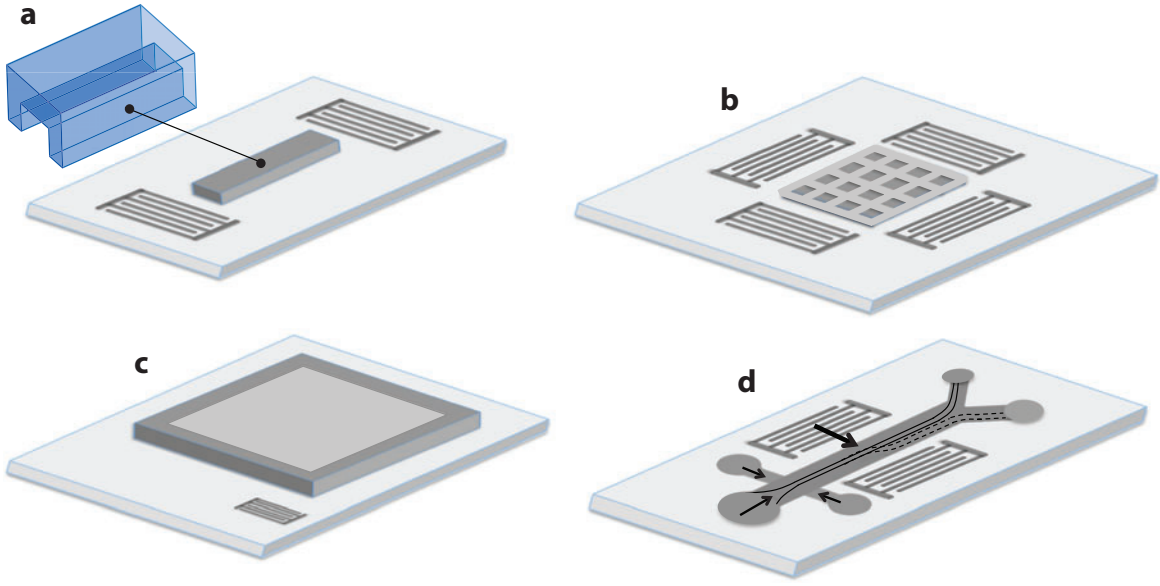

Figure 4

Schematic depiction of the various surface acoustic wave (SAW) fluid actuation and manipulation concepts (not to scale). (*a*) Fluid transport through a polydimethylsiloxane (PDMS) microchannel, open at both ends, placed atop the SAW substrate along the longitudinal axis of SAW propagation (Cecchini et al. 2008). (*b*) This was later extended to a 5 × 5 square PDMS microchannel grid with multiple interdigital transducer (IDTs), each being located at the entry and exit points of the grid (Masini et al. 2010). (*c*) Fluid transport around a closed PDMS microchannel loop placed atop the SAW substrate (Langelier et al. 2012, Schmid et al. 2012). (*d*) Fluid switching mechanism with two transverse IDTs flanking a microchannel. The central hydrodynamically focused stream is deflected into a bifurcated outlet downstream with the transverse SAW by imparting a direct acoustic force on the liquid-liquid interface or as a consequence of acoustic streaming induced in the coflowing laminar streams (Franke et al. 2010).

and exit points of the grid (**Figure 4*b***) (Masini et al. 2010). By controlling selected IDTs, one can cause the liquid to turn at right angles at the desired grid junctions or even to split the flow at an intersection. Because of the trigonal anisotropy of single-crystal lithium niobate and the almost ubiquitous use of the 127.86° *Y*-rotated, *X*-propagating cut for making SAW devices, the crossflow along the *y* axis is significantly weaker than the flow along the *x* axis. The open channels also pose significant disadvantages, in terms of the susceptibility of the liquid to evaporation, the nonuniform contact line advancing speeds due to contact line instabilities, and pinning and hysteresis in the presence of surface impurities. The difficulties in maintaining a uniform advancing speed are also compounded by the atomization of the meniscus front and its coalescence with the deposited droplets. Schmid et al. (2012) subsequently demonstrated a closed-circuit PDMS microchannel pump that circumvents these limitations (**Figure 4*c***). The same racetrack loop was used several times in succession for microfluidic cell-cell, cell-particle, and cell-surface interaction studies (Fallah et al. 2010, Fillafer et al. 2009, Schneider et al. 2008a) and to invoke the shear stretching of the von Willebrand factor fibers discussed in Section 3.1.

Liquid interfaces in coflowing laminar streams within a straight PDMS channel may also be manipulated by placing the IDTs transverse to the channel in a setup similar to that of Shi et al. (2009b) and that depicted in **Figure 2*c***, except employing traveling SAWs (**Figure 4*d***) (Franke et al. 2010). In this case, however, the authors used the transverse SAW from the transverse IDTs to deflect the central hydrodynamically focused stream. Cells flowing within the central stream

can then be sorted into the branches of a downstream channel bifurcation. In this case, the acoustic radiation force on the cells was sufficiently small—a consequence of the choice of frequency such that the cell's size is below the crossover size at which the drag force on the cell dominates (Rogers et al. 2010). As a result, the cells are enslaved to the hydrodynamics and follow the trajectory of the carrier stream. It is not clear whether the deviation of the stream arises as a consequence of SAW-induced streaming as the authors claim or whether it arises as a consequence of the direct acoustic force on the particles themselves. We believe that the latter is perhaps more plausible based on the results of a related study employing the same setup to deflect individual drops in an immiscible fluid continuum flowing within the microchannel (Franke et al. 2009).

As with Cecchini et al. (2008) and the channels described in Section 2 for continuous-flow particle separation, PDMS channels in all of these designs were mounted on the SAW substrate to compose a partial or complete fluid enclosure. Nevertheless, the use of PDMS atop the substrate is a major limitation despite its fabrication ease and low costs because of the acoustically lossy nature of elastomeric materials, which leads to excessive absorption of the acoustic radiation, thus resulting in excessive heating, undesirable resonance or reflection, high power consumption, and hence low efficiency (Langelier et al. 2012). To circumvent this, Tan et al. (2009a) laser-ablated microchannels into the SAW substrate along the crystal orientation axis (**Figure 2*d***) such that the SAW travels along the sides of the microchannel. The leakage of the sound field into the fluid at the Rayleigh angle along the channel side walls then results in acoustic streaming, which drives fast unidirectional fluid actuation in the microchannel in the direction of SAW propagation, if the channel width typically matches the sound wavelength in the fluid, or induces an oscillatory flow, which can be exploited for micromixing if the channel width is considerably larger than the sound wavelength.

As it may often be impractical to expand or contract the channel to pump and mix on a single device, reversible switching between transport and mixing can be achieved along the same microchannel by switching between the fundamental and harmonic frequencies employing a single IDT configuration using the fundamental and harmonic overtone resonance frequencies (Tan et al. 2010b). Tan et al. (2009c) also demonstrated particle sorting into downstream channel bifurcations while pumping in these microchannels embedded in the SAW device by driving double-aperture focusing IDTs. A particle traveling along the microchannel experiences an asymmetric acoustic radiation force that deflects it to one side of the microchannel when one of the two IDTs is activated. The standing wave across the channel can be deliberately suppressed by employing an anechoic trapezoidal channel with channel side walls that have different slopes, leaving only a traveling wave across the channel that presents a direct acoustic force on the particle from one side or the other as desired. The anechoic form of the channel cross section avoids the standing acoustic waves in the fluid bulk as discussed in Section 2. One can then also introduce streaming and hence flow through the microchannel to facilitate particle transport.

The microchannels in Tan et al. (2009a,c, 2010b) were nevertheless open to atmospheric conditions, suffering from the same drawbacks of evaporation and sample contamination of other open-channel or planar drop devices. There had been longstanding challenges associated with the bonding of piezoelectric materials, including a need to accommodate electrodes and the intolerance of wafer bonding processes, particularly the high temperatures that lead to charging, fracture, and even depolarization of the piezoelectric material. Therefore, closing the channels with nonacoustically lossy materials such as glass and silicon has only recently been made possible. Langelier et al. (2012) first aligned a glass cover slide and brought it into contact with the SAW substrate with the aid of a compressional load. A low-viscosity epoxy resin was then wicked into the microscopic gap between the surfaces via capillary pressure and then cross-linked under UV light to form a thin, rigid adhesive bond between the surfaces. The transmission of SAWs along

THE REYNOLDS NUMBER: HYDRODYNAMIC, STREAMING, AND ACOUSTIC REPRESENTATIONS

A universal issue in treating acoustic fields in microfluidics is the appropriate use of the Reynolds number, Re. The hydrodynamic Reynolds number is typically less than 1 in most microfluidics devices. This form, however, makes use of the Eulerian fluid velocity, which is inappropriate for situations incorporating acoustics. The streaming Reynolds number is the typical and far more useful representation in these cases, using instead the Lagrangian fluid velocity, incorporating the vibration velocity induced by the passage of the acoustic wave. The need for a distinction is apparent from the literature in this area, with researchers showing turbulent flow, mixing, enhanced diffusion, and other such phenomena in microfluidics devices in which typically the hydrodynamic Re $\leq$ 1. Unfortunately, there are various definitions of the streaming Reynolds number, and some call this number the acoustic Reynolds number (which is actually a fluid property and constant) (see the glossary in Friend & Yeo 2011).

the bonded substrates appeared to improve with thinner bond interfaces, particularly when the bond was made to be far thinner than the wavelength of the SAW, which was achieved through higher compressional loading placed on the interface before instilling the epoxy. This technique breaks down for very high-frequency SAWs, for which the wavelength becomes comparable to the micrometer-order thickness of the bond. Langelier et al. (2012) demonstrated that a SAW closed-loop microchannel pump bonded using this technique achieved similar backpressures in comparable microchannel dimensions but with a tenfold decrease (10 dB) in the requisite energy transmission compared to that of the PDMS-bonded microchannel pump of Schmid et al. (2012).

3.3. Microcentrifugation

To date, sample preconcentration remains a considerable challenge in microfluidics, and there have been few viable solutions, let alone attempts, to drive efficient centrifugation at small scales. Fortunately, as seen above, the fluid-structural coupling associated with SAW microfluidics is sufficiently effective to drive flows to have Reynolds numbers beyond unit order (see the sidebar The Reynolds Number: Hydrodynamic, Streaming, and Acoustic Representations). Driving azimuthal fluid recirculation in microcentrifugation, however, requires the ability to break the symmetry of the planar SAW wave across a drop or fluid confined in a circular chamber. Li et al. (2007b) were the first to report several methods to systematically and reliably break the symmetry of the planar wave and therefore induce fluid rotation across the entire drop (**Figure 5**), by offsetting the drop such that part of it lies outside the radiation pathway, incorporating a slanted cut at the device edge such that the reflections at the edges are asymmetric across the device, or absorbing part of the energy of the wave at the reflector IDT.

Mixing is notoriously difficult in microfluidic devices, particularly because the low Reynolds numbers do not permit turbulent mixing vortices. As such, both passive and active micromixing strategies have been pursued to introduce chaotic advection into the system to efficiently stretch and fold the fluid element striations, thereby increasing the interfacial area and hence reducing the diffusion timescale. Given the relatively large Reynolds numbers typical of SAW-driven microfluidics (Re $\sim$ 10–100), SAW-driven advective flows are therefore particularly efficient at driving chaotic micromixing (Alghane et al. 2012a,b; Frommelt et al. 2008; Shilton et al. 2011b) whether through oscillatory flows in microchannels (Tan et al. 2009a, 2010b) or through azimuthal microcentrifugal flows in drops or cylindrical microchambers (Li et al. 2007b, Shilton et al. 2008)

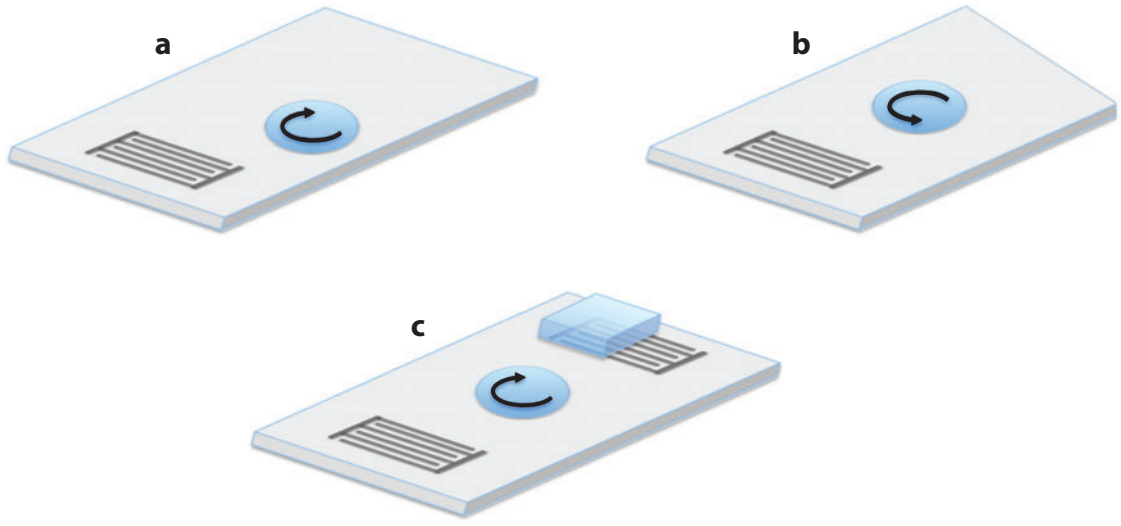

Figure 5

Schematic depiction of various schemes for symmetry breaking of a surface acoustic wave to drive microcentrifugation (Li et al. 2007b). (*a*) Offset placement of the drop such that only part of the drop lies in the radiation pathway. (*b*) Asymmetric wave reflection at the slanted edge of the device. (*c*) Asymmetric wave reflection via wave absorption on one-half of the reflector interdigital transducer.

(**Figure 6*a***). Indeed, such efficient mixing (Tseng et al. 2006), possibly aided by modest sample heating by the leakage of the SAW into the fluid, has led to a notable enhancement in chemical and biochemical reaction yields and has significantly reduced reaction times (Kulkarni et al. 2009). For example, a standard overnight in-gel tryptic digestion procedure can be reduced to a mere 30 min with a SAW while maintaining excellent and reproducible protein coverage (Kulkarni et al. 2010). However, it has yet to be ascertained whether activation energy barriers are overcome via temperature or compressional effects. Such mixing has also been shown to lead to enhancement in sensor detection (Ducloux et al. 2010). SAW-driven drop mixing was reported by Li et al. (2012b), who further combined the SAW platform with an electrode array to take advantage of the finer ability for drop manipulation (e.g., translation, splitting, and merging) with electrowetting. A scheme to detect the drop position using surface-horizontal SAWs (see, e.g., Kondoh et al. 2003) was also included.

In contrast to dispersing solutes through chaotic advection, particle and bioparticle suspensions can be concentrated for partitioning, separation, and sorting within a drop placed on a SAW device as a microcentrifuge, mimicking conventional laboratory-based centrifugation at a far smaller scale. **Figure 6*b*** shows the rapid concentration of submicrometer fluorescent particles under a strong microcentrifugation flow induced within a drop or cylindrical microchamber by the SAW in under 1 s (Li et al. 2007b, Shilton et al. 2008). This is extremely useful, for example, for the separation of red blood cells (Li et al. 2007b) from plasma for subsequent downstream processing, analysis in microfluidic point-of-care diagnostic devices, or for sample preconcentration for subsequent downstream detection, circumventing the low-detection sensitivity limitations that typically plague biosensor technology to date. In addition to allowing detection with greater sensitivity, the rapid convective flow overcomes diffusional limitations in the transport of the analyte to the capture probes immobilized on the surface, thus enhancing the detection speed, and also can aid in shearing unbound or nonspecifically bound targets to amplify the selectivity of the detection.

Surface-horizontal surface acoustic wave: a compressional-shear coupled wave with motion entirely in the plane of the surface; the compression is along the axis of travel

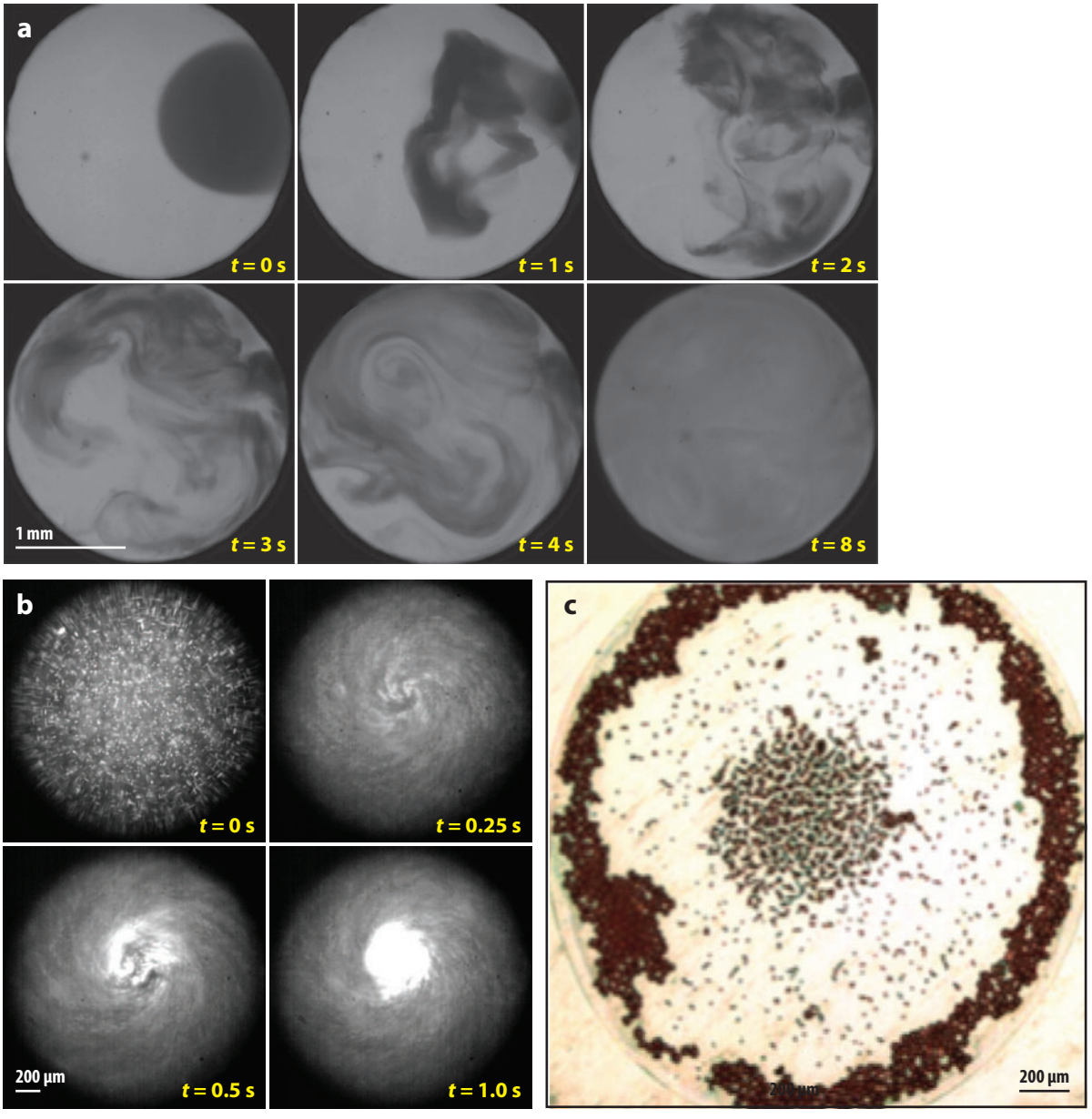

Figure 6

Microcentrifugation driven by surface acoustic waves in a millimeter-dimension microchamber demonstrating (*a*) efficient micromixing (Shilton et al. 2011b), (*b*) rapid concentration of 500-nm fluorescent particles (Shilton et al. 2008), and (*c*) size-dependent particle sorting between pollen (12–13 μm; *center*) and polystyrene microparticles (31 μm; *periphery*) (Rogers et al. 2010).

The particles concentrate within the microcentrifugation flow via three possible mechanisms: on the free surface of the drop by shear-induced diffusion (Li et al. 2007b, Shilton et al. 2008), within the bulk of the drop owing to drop-scale secondary meridional vortices that convect the particles to a pseudoconverging stagnation point in the center of the drop (Raghavan et al. 2010), or sound wavelength-scale segregation due to the BAW in the fluid.

Given the distinct particle size scaling of the acoustic radiation force and the drag force discussed in Section 2, these competing forces, which act on a particle suspended in the flow in opposing manners, can be exploited to discriminate, sort, and partition particles based on their size in the microcentrifugation flow (Rogers et al. 2010). Given that the drag force dominates below a frequency-dependent crossover particle size, particles with dimensions smaller than the crossover appear to concentrate in the center of the drop, whereas particles with dimensions above the crossover are seen to be driven to the periphery of the drop by the direct acoustic force that dominates the fluid drag above the critical crossover size of the particle. This was demonstrated to separate synthetic particles from pollen in the SAW microcentrifuge (**Figure 6*c***).

Furthermore, the azimuthal microcentrifugation flow on the SAW device can be exploited to drive the rotation of impellers housed in microchambers filled with the rotating fluid and arranged such that it is exposed to asymmetric SAW radiation through one of the schemes illustrated in **Figure 5** (Shilton et al. 2012) or discs placed atop the rotating fluid (Shilton et al. 2011a). Rotation speeds of the order of 1,000 rpm and up to 10,000 rpm with torques of the order of 100 nN-m, depending on the viscosity of the fluid, have been reported for a range of impeller and disc designs between 200 nm and 5 mm in diameter. In the case of the impellers or discs in the microchambers, the rotation is driven directly by contact with the SAW vibration on the substrate without requiring a fluid couplant by exploiting adhesive stiction with the impeller or disc surface (Shilton et al. 2012, Tjeung et al. 2011). The bane of microelectromechanical systems is made useful here: Such solid-state actuation is desirable when the presence of a fluid couplant is inconvenient and acts to retain the rotor in place both when operating and when off.

Finally, microfluidic features such as microchannels and reaction/separation microchambers can be patterned onto the discs to carry out a variety of chip-scale microcentrifugal operations, not unlike the concept of a lab on a compact disc (CD) (Madou et al. 2006). The distinction, however, is the small size of the discs in the SAW-driven miniature lab-on-a-disc (miniLOAD) platform (Glass et al. 2012), which are one to two orders of magnitude smaller than the CD structures (**Figure 7**) and consequently more convenient to use and discard, a necessity in hygienically sensitive operations such as medical diagnostics. In addition, the entire miniLOAD platform, which comprises the SAW substrate together with the portable driver circuit (**Figure 1**), is integrated within a battery-powered, miniature handheld platform, unlike the lab on a CD, which requires a large laboratory benchtop CD player to drive the bulk rotation of the CD. In the initial proof of concept, Glass et al. (2012) demonstrated various microfluidic operations, such as capillary-based valving, micromixing, and size-dependent particle separation, on the miniLOAD platform. Alghane et al. (2012b) also explored the behavior of confined acoustic streaming relevant to the action of the fluid on the disc by examining the scaling effects of the fluid height and their coupling to the SAW-induced streaming within.

4. JETTING

If the streaming in a drop is confined and directed toward the drop's free surface with sufficient inertia to overcome the capillary stress and hence deform the drop interface, it is possible to extrude a thin liquid jet that emanates from the free surface of the drop; this was first illustrated by Shiokawa et al. (1990). Tan et al. (2009b) later showed examples of controlled jetting in which

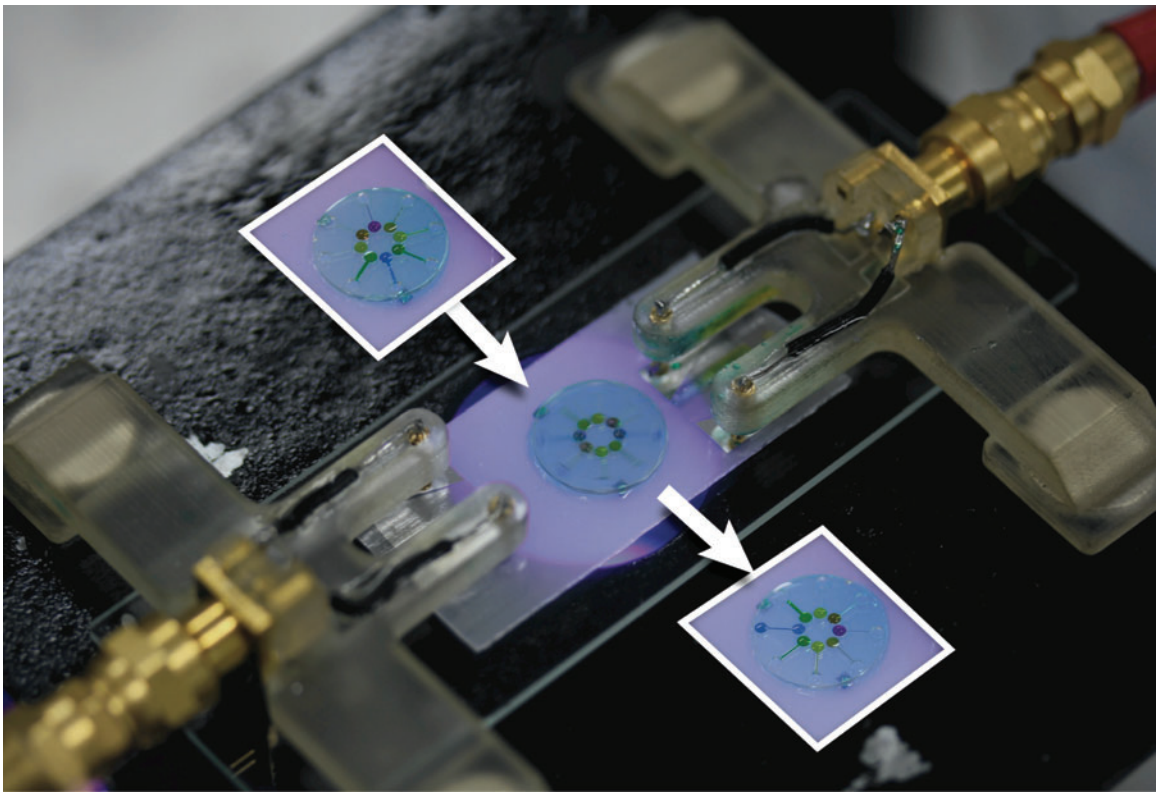

Figure 7

The miniature lab-on-a-disc centrifugal microfluidics platform (Glass et al. 2012). A typical capillary valving operation on the platform is shown.

a millimeter-sized drop deforms into an elongated liquid column that extends over centimeters in length without requiring nozzles or orifices. To concentrate the energy under the drop and hence drive inertial streaming that converges from the side of the drop vertically toward the drop's free surface to deform the drop into a jet, Tan et al. (2009b) employed a pair of elliptical focusing single-phase unidirectional transducers (Shilton et al. 2008), driving two coincident SAWs from both ends of the substrate such that they converge at a focal point underneath the drop. As shown in **Figure 8*a***, the jet subsequently suffers from the usual Rayleigh-Plateau instability and either pinches off to form a single droplet or breaks up to form multiple droplets, depending on the jet's Weber number, $\mathrm{We} \equiv \rho U_j^2 R_j/\gamma$, where U_j, R_j, ρ, and γ are the jet velocity and radius and the fluid's density and surface tension, respectively. This defines the relative magnitude between the destabilizing inertial stress and the stabilizing capillary stress that in turn describes the jet's behavior.

Bhattacharjee et al. (2011) employed SAW jetting to extend a pendant drop on an inverted substrate such that it formed a liquid bridge with a second substrate beneath it (**Figure 8*b***). They then showed that the capillary thinning of the Newtonian liquid bridge followed the expected behavior for viscous fluids undergoing surface-tension-driven necking in which the neck radius decreases linearly until breakup occurs, thus demonstrating the SAW-driven microfluidic liquid bridge platform, termed the Acoustics Driven Microfluidic Extensional Rheometer (ADMiER), as

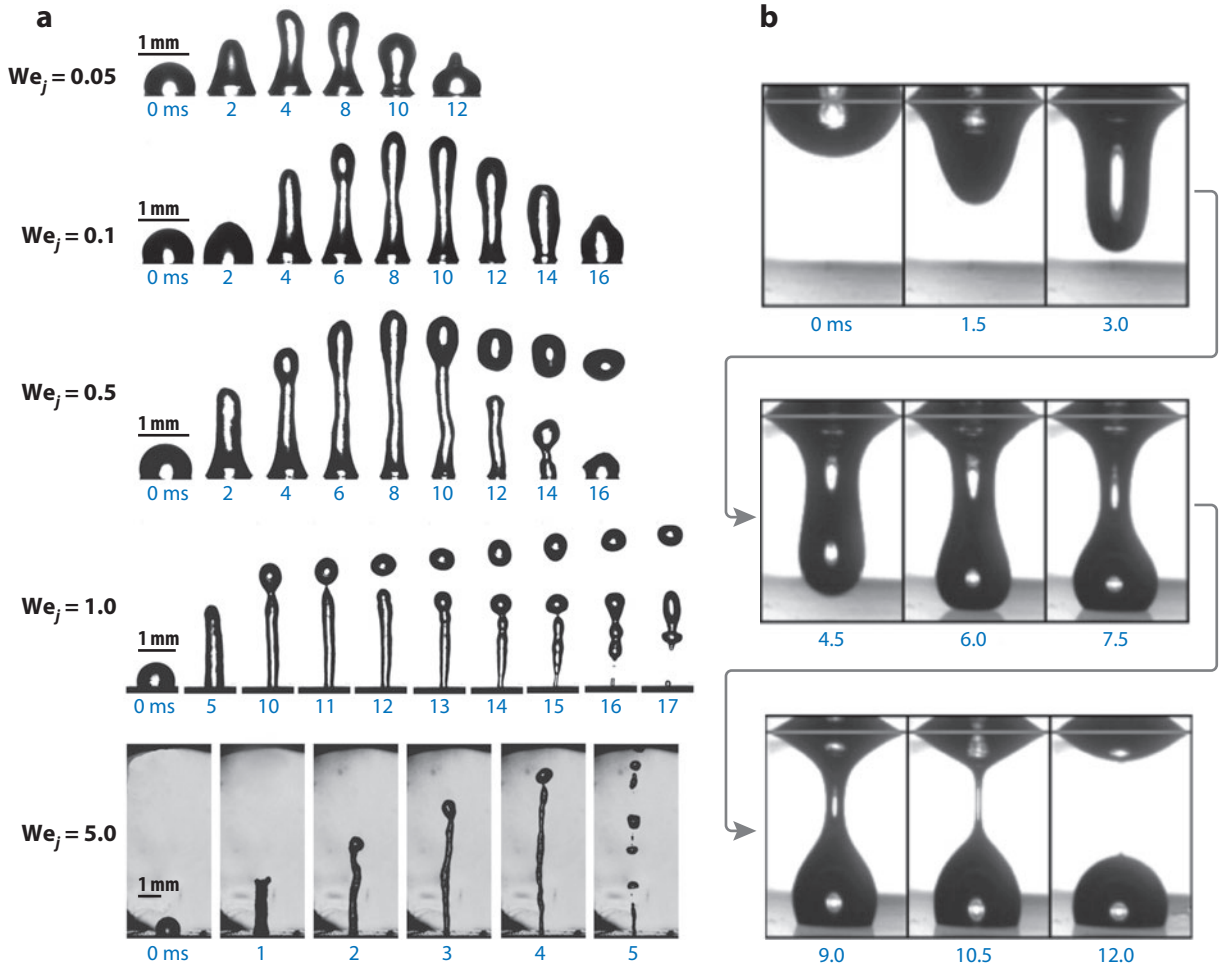

Figure 8

Surface acoustic wave (SAW) jetting. (*a*) Time-series images of the liquid jets and their subsequent breakup to form single or multiple droplets as a function of the Weber number, We (Tan et al. 2009b). (*b*) Time-series images showing the downward jetting of pendant drops with the SAW to form liquid bridges connecting a second bottom substrate. The subsequent thinning behavior of the liquid bridge is used to characterize the extensional behavior of Newtonian and viscoelastic fluids (Bhattacharjee et al. 2011).

a reliable rheometric tool for examining the evolution of fluid microstructures under elongation. A significant advantage of the ADMiER platform over the commonly employed capillary breakup elongation rheometry (CaBER) technique is the possibility of circumventing CaBER's limitation in forming capillary bridges of fluids with a viscosity below 70 mPa·s, which break up quicker (<50 ms) than the CaBER is able to form them. The ADMiER approach, however, is able to form a stable fluid bridge in just 0.1–10 ms. For the first time, therefore, one can carry out extensional rheometry of low-viscosity fluids such as water. Furthermore, the capillary thinning of viscoelastic liquid bridges followed the expected exponential thinning behavior in the elastocapillary dominant regime, thus allowing the measurement of the viscoelastic relaxation time, which is a clear signature of polymer-induced elasticity.

CAPILLARY WAVES AND NEBULIZATION

Capillary waves and their breakup to form droplets have been features of ultrasound technology for at least 40 years, with ultrasonic nebulizers widely available for medication and mist generation. A SAW is an effective means for generating atomized mists via capillary wave breakup, although it forms droplets possessing a size not correctly predicted by classical theories such as those used by Lang (1962). Indeed, why capillary waves appear at all at a fluid interface when the fluid bulk is excited by 10-MHz-order acoustic waves is an important question. By exciting the fluid interface, Blamey et al. (2013) demonstrated in a recent study the presence of capillary wave turbulence, a broadband Rayleigh-Jeans cascade from the fundamental capillary wave mode at frequencies of the order of 100 Hz to 1 MHz. The capillary wave train was formed from turbulence induced by the acoustic streaming. However, it remains an open question as to what drives the droplet size from such a broadband response.

5. ATOMIZATION

At higher powers, typically of the order of 1 W, the acceleration induced by the SAW increases to the order of 10^8 m^2/s, providing sufficient energy coupled through the streaming in a sessile drop to destabilize its interface, leading to its subsequent breakup to form 1-μm-order aerosol droplets (Chono et al. 2004, Kurosawa et al. 1995, Qi et al. 2008). The underlying physical phenomenon that gives rise to atomization through capillary wave breakup is surprisingly complex (Blamey et al. 2013) (see the sidebar Capillary Waves and Nebulization). Regardless, such an ability to produce a fine mist of monodispersed micrometer-dimension aerosol droplets with input powers that can still be generated using a battery-operated portable driver circuit coupled to a miniature chip-scale SAW substrate (**Figure 1**) constitutes a powerful tool for many applications involving aerosol production.

As one example, the SAW atomization platform has the potential to revolutionize pulmonary drug delivery with a means to efficiently deliver a uniform distribution of aerosolized drug with aerodynamic droplet diameters in the 1–5-μm range to target the deep lung region, all within a miniaturized, low-cost handheld platform (Qi et al. 2009). Unlike inhalers, which require hand and breath coordination, and hence training on proper usage, which leads to poor compliance with infants and children, the specific amount of drug delivered can be adjusted such that the administered dose can be tuned to the physiological profile (age, gender, size, disease severity) of a particular patient (Yeo et al. 2010b). Furthermore, there is a significant advantage of SAW atomization over ultrasonic nebulization beyond the capability for miniaturization: The cavitation and shear damage commonly inflicted on large therapeutic molecules such as peptides, proteins, DNA, and stem cells during ultrasonic nebulization are typically negligible at the considerably higher frequencies (10 MHz and above) of operation associated with SAW atomization (Yeo et al. 2010b). Because the onset of cavitation is dependent on the square of the frequency of the acoustic irradiation (Friend & Yeo 2011), cavitation is essentially absent at higher-megahertz-order frequencies. Moreover, the characteristic timescales at high frequencies are considerably shorter than those associated with molecular hydrodynamic shear relaxation and with molecular degradation or cell damage (Li et al. 2009, Qi et al. 2010).

Qi et al. (2009) demonstrated the miniaturized SAW atomization platform for the pulmonary delivery of asthmatic steroids. They reported up to 80% in vitro lung dose efficiencies, significantly higher than the 10–30% obtained with commercially available inhalers and nebulizers. The SAW atomizer is nevertheless a generic platform: Any drug solution that can be atomized can potentially

be delivered by inhalation. Indeed, there have been recent in vitro and in vivo studies that show good therapeutic efficacy with monoclonal antibodies and DNA-based vaccines (A. Rajapaksa, J. Ho, A. Qi, T.H. Nguyen, M. Tate, et al., manuscript under review). In the latter, in sheep dosed with plasmid DNA encoded with an H1N1 influenza vaccine sequence delivered via inhalation with SAW atomization, the systemic antibody response showed results comparable with those obtained with vaccines delivered parenterally (A. Rajapaksa, J. Ho, A. Qi, T.H. Nguyen, M. Tate, et al., manuscript under review).

Polymeric and protein nanoparticles can also be simply and rapidly synthesized by atomizing a solution of polymeric excipient (Alvarez et al. 2008b, Friend et al. 2008, Kim et al. 2005). The evaporation of the solvent in-flight as the droplets leave the free surface of the parent drop then leaves behind a 100–200-nm-diameter solidified spherical cluster comprising sub-50-nm particle aggregates, arising as a consequence of spinodal phase separation driven by nonuniformity in the evaporation (Friend et al. 2008). Furthermore, peptides, proteins, DNA, and other therapeutic molecules can be encapsulated within the polymer shell (Alvarez et al. 2009). If the polymer is biocompatible and biodegradable, such particles then constitute a method for uniform and controlled release of the drug over prolonged periods determined by the polymer in vivo degradation timescale. The ability of the SAW atomizer here presents a unique opportunity for simultaneous synthesis and encapsulation together with in situ pulmonary delivery at the point of need, which could potentially address problems associated with the stability and degradability of the nanoparticles during storage or transport, particularly in the developing world, where problems associated with extreme heat or the breaking of the cold chain due to a lack of refrigeration facilities are common. In addition, solvent evaporation as the polymer solidification method typically leads to higher encapsulation efficiencies compared to other synthesis and encapsulation methods that rely on solvent extraction (i.e., polymer desolvation), as the solvent evaporates much more quickly than the aqueous phase containing the therapeutic, thus trapping it within the fast solidifying polymer shell. Furthermore, Qi et al. (2011) demonstrated the possibility of drug encapsulation within nanoparticles comprising multiple layers of polymers by simply suspending the solidified polymer nanoparticle within a complementary polymer solution and reatomizing this solution. Every successive repetition of this atomization-suspension cycle adds an additional polymer layer over the existing nanoparticle. Qi et al. (2011) showed good stem cell–transfection efficiency with plasmid DNA encapsulated nanoparticles with up to eight alternating layers of chitosan (or polyethyleneimine) and carboxymethyl cellulose.

Atomization can also be carried out from the liquid meniscus that forms at the edge of a paper strip brought in contact with the SAW device (Qi et al. 2010). Atomization from paper has several advantages. At the paper edge, it generates a negative pressure gradient that draws liquid rapidly through the paper such that it acts like a capillary wick, therefore constituting a simple, low-cost, disposable fluid delivery option connecting the SAW device with a liquid reservoir. There are two further advantages associated with the use of paper delivery for SAW atomization. As opposed to atomization from a sessile drop, SAW excitation tends to draw out a counterpropagating (i.e., in the direction opposite to the SAW propagation direction) thin-film meniscus (Manor et al. 2012, Rezk et al. 2012a) that forms at the edge of the paper substrate in contact with the hydrophilic lithium niobate substrate; the thin meniscus is defined by the thinness of the paper. The small aspect ratio of the advancing film from which atomization ensues not only facilitates the generation of the smaller 1–5-μm droplet sizes necessary for optimum inhalation therapy, but also allows the possibility of generating submicrometer droplet dimensions given the dependence of the interfacial instability wavelength and hence the ejected droplet size on the aspect ratio of the parent liquid source (Collins et al. 2012, Qi et al. 2008). Furthermore, the paper can act as a filter matrix that allows analyte preseparation prior to subsequent on-chip operations or atomization (Ho et al.

2011). Illustrating the use of this approach on cell cultures, Bllaci et al. (2013) showed that live islets of Langerhans can be irradiated with SAWs and the fluids within the intercellular matrix of these islets can be nebulized to examine the key factors in the onset of diabetes with matrix-assisted laser desorption/ionization mass spectrometry.

Rayleigh surface acoustic wave: a compressional-transverse coupled wave propagating along the surface of a material; the compression is along the axis of travel

Sezawa surface acoustic wave: the first harmonic of the Rayleigh surface acoustic wave; found in layered media in which the thin film has a slower speed of sound than the substrate

In fact, paper can be employed in place of conventional silicon or elastomeric microfluidic substrates to carry out a wide range of assays—as a more versatile and sophisticated version of its ubiquitous predecessor, the home pregnancy test strip. Paper-based microfluidics has received widespread attention of late because of its promise of portable, inexpensive, and reliable point-of-care diagnostics, especially for use in developing nations (Li et al. 2012a, Martinez et al. 2010). Rezk et al. (2012b) demonstrated the use of SAW atomization for driving fast and uniform fluid flow and mixing in paper networks to overcome limitations associated with microscale nonuniformities present in paper and consequent irregularities in passive capillary transport through the tortuous channels of the paper. Atomization is also a powerful tool for the extraction of analytes and biomolecules out of the paper substrates for subsequent analysis and detection (Qi et al. 2010). For example, SAW atomization has been employed as a simple, yet effective ionization source to interface microfluidic chips and paper-based microfluidics with mass spectrometry, achieving detection limits comparable with those obtained with inductively coupled plasma mass spectrometry, which is considered the gold standard for trace quantities of toxic heavy metals (Heron et al. 2010, Ho et al. 2011). A further advantage of SAW atomization as an ionization source is its ability to produce ions with lower internal energies than electrospray ionization, therefore leading to lower molecular fragmentation tendencies (Huang et al. 2012), thus enabling the application of SAW atomization for the analysis of, for instance, amphiphilic and labile molecules with aggregation tendencies, such as lipid samples (Yoon et al. 2012).

6. ACTUATION ON THIN-FILM DEVICES

In addition to piezoelectric substrates, it is also possible to generate SAWs on piezoelectric thin films such as zinc oxide (ZnO) and aluminum nitride, thus allowing the possibility of carrying out SAW-driven microfluidics on conventional silicon substrates, on which a thin film with a 1-μm-order thickness is deposited. To drive acoustic streaming in a drop, investigators employed the first harmonic of Rayleigh SAWs (i.e., the Sezawa SAW mode) that exists in these structures when the ratio of the film thickness to wavelength is around unity. The streaming velocities obtained were comparable with or slightly higher than those obtained with Rayleigh SAWs generated on lithium niobate at the same frequency (Du et al. 2008). Drop transport driven by both Rayleigh SAWs and Sezawa SAWs was subsequently demonstrated by patterning a silane layer atop the ZnO film to render the film hydrophobic, again with translation velocities of the order of 1 cm/s, similar to those obtained on lithium niobate devices discussed in Section 3.1 (Du et al. 2009). Brief allusion was made to other fluid manipulation schemes demonstrated on lithium niobate devices discussed above, such as particle manipulation (Section 2) and atomization (Section 5) (Fu et al. 2012a,b), although a thorough investigation to show careful control of their behavior has yet to be reported. Fu et al. (2010) have provided an in-depth discussion on the material properties that support good acoustic wave transmission in thin ZnO films together with an overview of various deposition methods. Recently, Fu et al. (2012a) showed a promising possible route to circumvent these limitations by depositing a ZnO thin film on a very smooth nanocrystalline diamond layer, which permitted the growth of the film along the *c*-axis orientation (i.e., the principal axis) of the crystal. Diamond was chosen not only because of its large elastic modulus and enhanced mechanical strength, but also especially for its fast sound propagation—in fact, diamond has the

highest sound speed of all materials—thus isolating the Sezawa wave energy to the piezoelectric thin film present atop the diamond and avoiding parasitic losses into the substrate.

7. SUPERSTRATE COUPLING

Hodgson et al. (2009) first demonstrated the possibility of transmitting the acoustic energy from the SAW into a glass superstrate mounted above the SAW device atop a fluid/gel coupling layer, thus presenting an opportunity for microfluidic operations to be conducted on a material conventionally used in fabrication instead of a piezoelectric substrate. The isolation of the working fluid from the piezoelectric substrate not only provides the option for disposability with cheaper materials and reuse of the SAW device, but also allows greater flexibility for chemical and biological functionalization and heating of surfaces that may otherwise be impractical or unsuitable.

Nevertheless, despite misunderstandings that have been repeated in subsequent literature, the manner in which the acoustic energy is coupled does not support the existence of a SAW in the superstrate—a Lamb wave is excited on the substrate in place of the SAW with roughly 50% transmission efficiency, as shown by Hodgson et al. (2009). Within, it has been shown that it is still possible to carry out microfluidic manipulations atop the superstrate similar to those driven by the SAW, such as drop translation and atomization, albeit at the expense of additional dissipative losses through the superstrate and the lower fluid-structural coupling efficiency of Lamb waves. In addition to drop translation and merging, Bourquin et al. (2010) later showed the potential for driving the same microcentrifugation processes for particle concentration discussed in Section 3.3. Symmetry breaking of the planar acoustic wave into the drop to drive the azimuthal recirculation was instead achieved using tIDTs. The width of the SAW generated by the application of a specific input frequency corresponding to a particular location along the tIDT aperture (and associated with the particular finger and gap width there) is much smaller than the drop dimension (Wu & Chang 2005). This finding was later employed to drive rapid convective mixing in the drop suspended with beads labeled with antibodies to facilitate antigen capture and subsequently to concentrate the beads onto the surface for binding with detection antibodies (Bourquin et al. 2011a). In addition, a wash step was also incorporated by sweeping the drop containing unbound beads away from the locality of binding to achieve more sensitive detection via fluorescence. Later work also used a similar setup for superstrate-based microcentrifugation for the release of DNA through lysis of the blood cells, and subsequent detection via amplification of specific malarial parasitic sequences using polymerase chain reaction (Reboud et al. 2012a).

To compose band gap and waveguide structures that can be exploited to filter, scatter, or reflect the Lamb waves, one can construct a phononic crystal lattice by patterning on the superstrate a regular periodic array of vacancy sites, circular holes, or posts, each with a diameter D corresponding to the IDT spacing and hence one-half the acoustic wavelength, with an array pitch p specified to give a fill fraction ($\pi D^2/4p^2$) of 0.5 (Khelif et al. 2004). This was demonstrated for shielding a sessile drop from part of the Lamb wave as an alternative symmetry-breaking measure to those discussed in Section 3.3 for driving azimuthal recirculation within the drop (Wilson et al. 2011) or for focusing the wave to drive jetting (Bourquin et al. 2011b) similar to that in Section 4 or atomization (Reboud et al. 2012b) similar to that in Section 5.

Finally, it is also possible to transmit acoustic energy into a superstrate without the use of a fluid/gel coupling layer. Johansson et al. (2012b) placed a fused silica superstrate atop an *X*-cut, *Z*-propagating lithium tantalate substrate, both with and without a 5-μm-thick SU-8 adhesive layer. The authors used the Stoneley interface waves generated between the piezoelectric substrate and the silica superstrate to align particles (Section 2) in a microchannel etched into the superstrate. The same group subsequently demonstrated a similar setup and particle alignment

strategy by bonding a glass superstrate on the SU-8 layer deposited above a lithium niobate chip (Johansson et al. 2012a). Unlike the case of Tan et al. (2009c) discussed above in Section 3.2, the trapezoidal channel they etched into the superstrate had side walls with similar slopes, and hence the standing BAW generated within the fluid channel required to align the particles was not suppressed. Nevertheless, the use of interface waves is an interesting development that may find much broader use in the future.

FUTURE ISSUES

1. Current approaches to acoustic streaming typically follow the classic approaches of Rayleigh, Nyborg, and Westervelt. They omit the treatment of streamwise acceleration and overlook the fact that the vibration velocity may substantially exceed the fluid velocity, each aspect invalidating the classic approach. Lighthill (1978) noted that for megahertz-order frequencies, even weak acoustic waves (~1 mW) are beyond the limits of the classic approach, exhibiting turbulence that results in fascinating phenomena (Blamey et al. 2013), but also indicating that a new method is needed.
2. Confined flow generation using acoustic streaming is a challenge because of the formation of standing waves in the fluid chamber. These interfere with the symmetry breaking necessary to form unidirectional flow with sufficient inertia to serve as a fluid or particle transport device. The use of SAW is helpful, but on mode conversion (Hodgson et al. 2009), the acoustic wave is no longer bound to the surface, with substantial losses throughout the system, particularly in devices constructed using soft lithography with PDMS. Although alternatives have been offered (Langelier et al. 2012), they are only stopgap solutions to the problem. The use of diamond and tungsten layers as acoustic reflectors, silicon and glass patterning, and fluid superstrate coupling will potentially help address these issues.
3. Interfacial dynamics is strongly coupled to the acoustic waves carried in the bulk of fluids. The deformation of a fluid interface causes changes in the acoustic wave field in the fluid bulk that can cause rapid fluid flow changes that are difficult to predict, let alone accommodate, in microfluidics devices. Better understanding of the dynamics, especially with very thin fluid films, is needed.
4. Fabrication improvements are vital to the integration of acoustic devices into microstructures for microfluidics. Although the mature discipline of soft lithography is suitable in limited cases, many applications require the incorporation of piezoelectric materials into silicon or glass structures. Even though this has been explored in piezoelectric inkjet printing with success (Wijshoff 2010), manipulating fluids with greater acoustic powers and acoustic streaming requires far more work.

DISCLOSURE STATEMENT

The authors are not aware of any biases that might be perceived as affecting the objectivity of this review.

ACKNOWLEDGMENTS

We thank Mar Alvarez, Dian Arifin, Jeremy Blamey, Nick Glass, Jenny Ho, Ketav Kulkarni, Sean Langelier, Haiyan Li, Ofer Manor, Amarin McDonnell, Aisha Qi, Rohan Raghavan, Anushi

Rajapaksa, Amgad Rezk, Richard Shilton, Ming Tan, and Ricky Tjeung for their hard work as students and postdoctoral associates in our group in this area. We also wish to extend our thanks to our collaborators for their contributions to the work reported here. We appreciate substantial funding for this work from the Australian Research Council via the Discovery, Fellowship, and Infrastructure grant schemes; the National Health and Medical Research Council via Development and Project grant schemes; the CSIRO; and the CASS Foundation. L.Y.Y. is grateful for an Australian Research Fellowship from the Australian Research Council, and J.R.F. appreciates the Vice-Chancellor's Senior Research Fellowship provided by RMIT University and the Senior Tech Fellowship provided by the Melbourne Centre for Nanofabrication.

LITERATURE CITED

Ai Y, Marrone BL. 2012. Droplet translocation by focused surface acoustic waves. *Microfluid. Nanofluid.* 13:715–22

Alghane M, Chen B, Fu Y, Li Y, Desmulliez M, et al. 2012a. Nonlinear hydrodynamic effects induced by Rayleigh surface acoustic wave in sessile droplets. *Phys. Rev. E* 86:056304

Alghane M, Chen B, Fu Y, Li Y, Luo J, Walton A. 2011. Experimental and numerical investigation of acoustic streaming excited by using a surface acoustic wave device on a 128° YX-$LiNbO_3$ substrate. *J. Micromech. Microeng.* 21:015005

Alghane M, Fu Y, Chen B, Li Y, Desmulliez MP, Walton A. 2012b. Scaling effects on flow hydrodynamics of confined microdroplets induced by Rayleigh surface acoustic wave. *Microfluid. Nanofluid.* 13:919–27

Alvarez M, Friend JR, Yeo LY. 2008a. Surface vibration induced spatial ordering of periodic polymer patterns on a substrate. *Langmuir* 24:10629–32

Alvarez M, Yeo LY, Friend JR. 2008b. Rapid generation of protein aerosols and nanoparticles via SAW atomization. *Nanotechnology* 19:455103

Alvarez M, Yeo LY, Friend JR, Jamriska M. 2009. Rapid production of protein-loaded biodegradable microparticles using surface acoustic waves. *Biomicrofluidics* 3:014102

Beyssen D, Le Brizoual L, Elmazria O, Alnot P. 2006. Microfluidic device based on surface acoustic wave. *Sens. Actuators B* 118:380–85

Bhattacharjee PK, McDonnell A, Prabhakar R, Yeo LY, Friend JR. 2011. Extensional flow of low-viscosity fluids in capillary bridges formed by pulsed surface acoustic wave jetting. *New J. Phys.* 13:023005

Blamey J, Yeo LY, Friend JR. 2013. Microscale capillary wave turbulence excited by high frequency vibration. *Langmuir* 29:3835–45

Bllaci L, Kjellström S, Eliasson L, Friend JR, Yeo LY, Nilsson S. 2013. Fast surface acoustic wave-matrix-assisted laser desorption ionization mass spectrometry of cell response from islets of Langerhans. *Anal. Chem.* 85:2623–29

Bok M, Li H, Yeo LY, Friend JR. 2009. The dynamics of surface acoustic wave-driven scaffold cell seeding. *Biotechnol. Bioeng.* 103:387–401

Bourquin Y, Reboud J, Wilson R, Cooper JM. 2010. Tuneable surface acoustic waves for fluid and particle manipulations on disposable chips. *Lab Chip* 10:1898–901

Bourquin Y, Reboud J, Wilson R, Zhang Y, Cooper JM. 2011a. Integrated immunoassay using tuneable surface acoustic waves and lensfree detection. *Lab Chip* 11:2725–30

Bourquin Y, Wilson R, Zhang Y, Reboud J, Cooper JM. 2011b. Phononic crystal structures for shaping fluids. *Adv. Mater.* 23:1458–62

Brunet P, Baudoin M, Matar OB, Zoueshtiagh F. 2010. Droplet displacements and oscillations induced by ultrasonic surface acoustic waves: a quantitative study. *Phys. Rev. E* 81:036315

Campbell C. 1998. *Surface Acoustic Wave Devices for Mobile and Wireless Communications*. New York: Academic

Cecchini M, Girardo S, Pisignano D, Cingolani R, Beltram F. 2008. Acoustic-counterflow microfluidics by surface acoustic waves. *Appl. Phys. Lett.* 92:104103

Chang H, Yeo LY. 2010. *Electrokinetically Driven Microfluidics and Nanofluidics*. Cambridge, UK: Cambridge Univ. Press

Chladni E. 1787. *Entdeckungen uber die Theorie des Klanges*. Leipzig, Ger.: Weidmanns, Erben und Reich

Chono K, Shimizu N, Matsui Y, Kondoh J, Shiokawa S. 2004. Development of novel atomization system based on SAW streaming. *J. Appl. Phys.* 43:2987–91

Collins DJ, Manor O, Winkler A, Schmidt H, Friend JR, Yeo LY. 2012. Atomization off thin water films generated by high-frequency substrate wave vibrations. *Phys. Rev. E* 86:056312

Ding X, Lin SCS, Kiraly B, Yue H, Li S, et al. 2012a. On-chip manipulation of single microparticles, cells, and organisms using surface acoustic waves. *Proc. Natl. Acad. Sci. USA* 109:11105–9

Ding X, Shi J, Lin SCS, Yazdi S, Kiralya B, Huang TJ. 2012b. Tunable patterning of microparticles and cells using standing surface acoustic waves. *Lab Chip* 12:2491–97

Doinikov AA. 1996a. On the radiation pressure on small spheres. *J. Acoust. Soc. Am.* 100:1231–33

Doinikov AA. 1996b. Theory of acoustic radiation pressure for actual fluids. *Phys. Rev. E* 54:6297–303

Doinikov AA. 2001. Acoustic radiation interparticle forces in a compressible fluid. *J. Fluid Mech.* 444:1–21

Du XY, Fu YQ, Luo JK, Flewitt AJ, Milne WI. 2009. Microfluidic pumps employing surface acoustic waves generated in ZnO thin films. *J. Appl. Phys.* 105:024508

Du XY, Fu YQ, Tan SC, Luo JK, Flewitt AJ, et al. 2008. ZnO film thickness effect on surface acoustic wave modes and acoustic streaming. *Appl. Phys. Lett.* 93:094105

Ducloux O, Galopin E, Zoueshtiagh F, Merlen A, Thomy V. 2010. Enhancement of biosensing performance in a droplet-based bioreactor by in situ microstreaming. *Biomicrofluidics* 4:011102

Durand Vidal S, Simonin JP, Turq P. 2001. Acoustophoresis revisited. 1. Electrolyte solutions. *J. Phys. Chem.* 99:6733–38

Eckart C. 1948. Vortices and streams caused by sound waves. *Phys. Rev.* 73:68–76

Fallah MA, Myles VM, Krüger T, Sritharan K, Wixforth A, et al. 2010. Acoustic driven flow and lattice Boltzmann simulations to study cell adhesion in biofunctionalized μ-fluidic channels with complex geometry. *Biomicrofluidics* 4:024106

Faraday M. 1831. On a peculiar class of acoustical figures; and on certain forms assumed by groups of particles upon vibrating elastic surfaces. *Philos. Trans. R. Soc. Lond.* 121:299–340

Fillafer C, Ratzinger G, Neumann J, Guttenberg Z, Dissauer S, et al. 2009. An acoustically-driven biochip: impact of flow on the cell association of targeted drug carriers. *Lab Chip* 9:2782–88

Franke T, Abate AR, Weitz DA, Wixforth A. 2009. Surface acoustic wave (SAW) directed droplet flow in microfluidics for PDMS devices. *Lab Chip* 9:2625–27

Franke T, Braunmuller S, Schmid L, Wixforth A, Weitz DA. 2010. Surface acoustic wave actuated cell sorting (SAWACS). *Lab Chip* 10:789–94

Friend JR, Yeo LY. 2010. Fabrication of microfluidics devices using polydimethylsiloxane. *Biomicrofluidics* 4:026502

Friend JR, Yeo LY. 2011. Microscale acoustofluidics: microfluidics driven via acoustics and ultrasonics. *Rev. Mod. Phys.* 83:647–704

Friend JR, Yeo LY, Arifin D, Mechler A. 2008. Evaporative self-assembly assisted synthesis of polymeric nanoparticles by surface acoustic wave atomization. *Nanotechnology* 19:145301

Frommelt T, Kostur M, Schäfer M, Talkner P, Hänggi P, Wixforth A. 2008. Microfluidic mixing via acoustically driven chaotic advection. *Phys. Rev. Lett.* 100:034502

Fu YQ, Garcia-Gancedo L, Pang HF, Porro S, Gu YW, et al. 2012a. Microfluidics based on ZnO/nanocrystalline diamond surface acoustic wave devices. *Biomicrofluidics* 6:024105

Fu YQ, Li Y, Zhao C, Placido F, Walton AJ. 2012b. Surface acoustic wave nebulization on nanocrystalline ZnO film. *Appl. Phys. Lett.* 101:194101

Fu YQ, Luo J, Du X, Flewitt A, Li Y, et al. 2010. Recent developments on ZnO films for acoustic wave based bio-sensing and microfluidic applications: a review. *Sens. Actuators B* 143:606–19

Galopin E, Beaugeois M, Pinchemel B, Camart JC, Bouazaoui M, Thomy V. 2007. SPR biosensing coupled to a digital microfluidic microstreaming system. *Biosens. Bioelectron.* 23:746–50

Glass NR, Shilton RJ, Chan P, Friend JR, Yeo LY. 2012. Miniaturized lab-on-a-disc (miniLOAD). *Small* 8:1880–88

Gor'kov L. 1961. On the forces acting on a small particle in an acoustic field within an ideal fluid. *Dokl. Akad. Nauk SSSR* 140:88–92

Guldiken R, Jo MC, Gallant ND, Demirci U, Zhe J. 2012. Sheathless size-based acoustic particle separation. *Sensors* 12:905–22

Hennig M, Neumann J, Wixforth A, Rädler JO, Schneider MF. 2009. Dynamic patterns in a supported lipid bilayer driven by standing surface acoustic waves. *Lab Chip* 9:3050–53

Heron S, Wilson R, Shaffer S, Goodlett D, Cooper J. 2010. Surface acoustic wave nebulization of peptides as a microfluidic interface for mass spectrometry. *Anal. Chem.* 82:3985–89

Hertz H. 1995. Standing-wave acoustic trap for nonintrusive positioning of microparticles. *J. Appl. Phys.* 78:4845–49

Ho J, Tan MK, Go DB, Yeo LY, Friend JR, Chang HC. 2011. Paper-based microfluidic surface acoustic wave sample delivery and ionization source for rapid and sensitive ambient mass spectrometry. *Anal. Chem.* 83:3260–66

Hodgson RP, Tan M, Yeo LY, Friend JR. 2009. Transmitting high power RF acoustic radiation via fluid couplants into superstrates for microfluidics. *Appl. Phys. Lett.* 94:024102

Hossenlopp JM. 2006. Applications of acoustic wave devices for sensing in liquid environments. *Appl. Spectrosc. Rev.* 41:151–64

Huang Y, Yoon SH, Heron SR, Masselon CD, Edgar JS, et al. 2012. Surface acoustic wave nebulization produces ions with lower internal energy than electrospray ionization. *J. Am. Soc. Mass Spectrom.* 23:1062–70

Jakubik WP. 2011. Surface acoustic wave-based gas sensors. *Thin Solid Films* 520:986–93

Jo MC, Guldiken R. 2012. Active density-based separation using standing surface acoustic waves. *Sens. Actuators A* 187:22–28

Johansson L, Enlund J, Johansson S, Katardjiev I, Wiklund M, Yantchev V. 2012a. Surface acoustic wave-induced precise particle manipulation in a trapezoidal glass microfluidic channel. *J. Micromech. Microeng.* 22:025018

Johansson L, Enlund J, Johansson S, Katardjiev I, Yantchev V. 2012b. Surface acoustic wave induced particle manipulation in a PDMS channel: principle concepts for continuous flow applications. *Biomed. Microdevices* 14:279–89

Khelif A, Choujaa A, Benchabane S, Djafari-Rouhani B, Laude V. 2004. Guiding and bending of acoustic waves in highly confined phononic crystal waveguides. *Appl. Phys. Lett.* 84:4400–2

Kim J, Yamagata Y, Takasaki M, Lee B, Ohmori H, Higuchi T. 2005. A device for fabricating protein chips by using a surface acoustic wave atomizer and electrostatic deposition. *Sens. Actuators B* 107:535–45

Kondoh J, Matsui Y, Shiokawa S. 2003. Identification of electrolyte solutions using a shear horizontal surface acoustic wave sensor with a liquid-flow system. *Sens. Actuators B* 91:309–15

Kong XH, Deneke C, Schmidt H, Thurmer DJ, Ji HX, et al. 2010. Surface acoustic wave mediated dielectrophoretic alignment of rolled-up microtubes in microfluidic systems. *Appl. Phys. Lett.* 96:134105

Kulkarni K, Friend J, Yeo LY, Perlmutter P. 2009. Surface acoustic waves as an energy source for drop scale synthetic chemistry. *Lab Chip* 9:754–55

Kulkarni K, Ramarathinam SH, Yeo LY, Purcell A, Perlmutter P. 2010. Rapid microscale in-gel processing and digestion of proteins using surface acoustic waves. *Lab Chip* 10:1518–20

Kundt A. 1866. Ueber eine neue Art akustischer Staubfiguren und über die Anwendung derselben zur Bestimmung der Schallgeschwindigkeit in festen Körpern und Gasen. *Ann. Phys. Chem.* 127:497–523

Kurosawa M, Watanabe T, Futami A, Higuchi T. 1995. Surface acoustic wave atomizer. *Sens. Actuators A* 50:69–74

Lang R. 1962. Ultrasonic atomization of liquids. *J. Acoust. Soc. Am.* 34:6–8

Länge K, Rapp BE, Rapp M. 2008. Surface acoustic wave biosensors: a review. *Anal. Bioanal. Chem.* 391:1509–19

Langelier SM, Yeo LY, Friend JR. 2012. UV epoxy bonding for enhanced SAW transmission and microscale acoustofluidic integration. *Lab Chip* 12:2970–76

Laurell T, Petersson F, Nilsson A. 2007. Chip integrated strategies for acoustic separation and manipulation of cells and particles. *Chem. Soc. Rev.* 36:492–506

Li H, Dasvarma A, Yeo LY, Friend JR, Traianedes K. 2009. Effect of surface acoustic waves on the viability, proliferation and differentiation of primary osteoblast-like cells. *Biomicrofluidics* 3:034102

Li H, Friend JR, Yeo LY. 2007a. A scaffold cell seeding method driven by surface acoustic waves. *Biomaterials* 9:647–56
Li H, Friend JR, Yeo LY. 2007b. Surface acoustic wave concentration of particle and bioparticle suspensions. *Biomed. Microdevices* 28:4098–104
Li H, Friend JR, Yeo LY. 2008. Colloidal island formation and erasure in a microfluidic system induced by surface acoustic wave radiation. *Phys. Rev. Lett.* 101:084502
Li X, Ballerini DR, Shen W. 2012a. A perspective on paper-based microfluidics: current status and future trends. *Biomicrofluidics* 6:011301
Li Y, Fu YQ, Brodie SD, Alghane M, Walton AJ. 2012b. Integrated microfluidics system using surface acoustic wave and electrowetting on dielectrics technology. *Biomicrofluidics* 6:012812
Lighthill J. 1978. Acoustic streaming. *J. Sound Vib.* 61:391–418
Lin SCS, Mao X, Huang TJ. 2012. Surface acoustic wave (SAW) acoustophoresis: now and beyond. *Lab Chip* 12:2766–70
Madou M, Zoval J, Jia G, Kido H, Kim J, Kim N. 2006. Lab on a CD. *Annu. Rev. Biomed. Eng.* 8:601–28
Manor O, Yeo LY, Friend JR. 2012. The appearance of boundary layers and drift flows due to high-frequency surface waves. *J. Fluid Mech.* 707:482–95
Martinez AW, Phillips ST, Whitesides GM, Carrilho E. 2010. Diagnostics for the developing world: microfluidic paper-based analytical devices. *Anal. Chem.* 82:3–10
Masini L, Cecchini M, Girardo S, Cingolani R, Pisignano D, Beltram F. 2010. Surface-acoustic-wave counterflow micropumps for on-chip liquid motion control in two-dimensional microchannel arrays. *Lab Chip* 10:1997–2000
McMillan EM. 1945. The synchrotron: a proposed high energy particle accelerator. *Phys. Rev.* 68:143–44
Meng L, Cai F, Chen J, Niu L, Li Y, et al. 2012. Precise and programmable manipulation of microbubbles by two-dimensional standing surface acoustic waves. *Appl. Phys. Lett.* 100:173701
Meng L, Cai F, Zhang Z, Niu L, Jin Q, et al. 2011. Transportation of single cell and microbubbles by phase-shift introduced to standing leaky surface acoustic waves. *Biomicrofluidics* 5:044104
Nam J, Lim H, Kim C, Kang JY, Shin S. 2012. Density-dependent separation of encapsulated cells in a microfluidic channel by using a standing surface acoustic wave. *Biomicrofluidics* 6:024120
Nam J, Lim H, Kim D, Shin S. 2011. Separation of platelets from whole blood using standing surface acoustic waves in a microchannel. *Lab Chip* 11:3361–64
Oberti S, Neild A, Quach R, Dual J. 2009. The use of acoustic radiation forces to position particles within fluid droplets. *Ultrasonics* 49:47–52
Orloff ND, Dennis JR, Cecchini M, Schonbrun E, Rocas E, et al. 2011. Manipulating particle trajectories with phase-control in surface acoustic wave microfluidics. *Biomicrofluidics* 5:044107
O'Rorke RD, Wood CD, Wälti C, Evans SD, Davies AG, Cunningham JE. 2012. Acousto-microfluidics: transporting microbubble and microparticle arrays in acoustic traps using surface acoustic waves. *J. Appl. Phys.* 111:094911
Pethig R. 2010. Review article—dielectrophoresis: status of the theory, technology, and applications. *Biomicrofluidics* 4:022811
Qi A, Chan P, Ho J, Rajapaksa A, Friend JR, Yeo LY. 2011. Template-free synthesis and encapsulation technique for layer-by-layer polymer nanocarrier fabrication. *ACS Nano* 5:9583–91
Qi A, Friend JR, Yeo LY, Morton DAV, McIntosh MP, Spiccia L. 2009. Miniature inhalation therapy platform using surface acoustic wave microfluidic atomization. *Lab Chip* 9:2184–93
Qi A, Yeo LY, Friend JR. 2008. Interfacial destabilization and atomization driven by surface acoustic waves. *Phys. Fluids* 20:074103
Qi A, Yeo LY, Friend JR, Ho J. 2010. The extraction of liquid, protein molecules and yeast cells from paper through surface acoustic wave atomization. *Lab Chip* 10:470–76
Raeymaekers B, Pantea C, Sinha DN. 2011. Manipulation of diamond nanoparticles using bulk acoustic waves. *J. Appl. Phys.* 109:014317
Raghavan R, Friend JR, Yeo LY. 2010. Particle concentration via acoustically driven microcentrifugation: microPIV flow visualization and numerical modelling studies. *Microfluid. Nanofluid.* 8:73–84
Rayleigh L. 1884. On the circulation of air observed in Kundt's tubes, and on some allied acoustical problems. *Philos. Trans. R. Soc.* 175:1–21

Reboud J, Bourquin Y, Wilson R, Palla GS, Jiwaji M, et al. 2012a. Shaping acoustic fields as a toolset for microfluidic manipulations in diagnostic technologies. *Proc. Natl. Acad. Sci. USA* 109:15162–67

Reboud J, Wilson R, Zhang Y, Ismail MH, Bourquin Y, Cooper JM. 2012b. Nebulisation on a disposable array structured with phononic lattices. *Lab Chip* 12:1268–73

Renaudin A, Chabot V, Grondin E, Aimez V, Charette PG. 2010. Integrated active mixing and biosensing using surface acoustic waves (SAW) and surface plasmon resonance (SPR) on a common substrate. *Lab Chip* 10:111–15

Renaudin A, Sozanski JP, Verbeke B, Zhang V, Tabourier P, Druon C. 2009. Monitoring SAW-actuated microdroplets in view of biological applications. *Sens. Actuators B* 138:374–82

Renaudin A, Tabourier P, Zhang V, Camart J, Druon C. 2006. SAW nanopump for handling droplets in view of biological applications. *Sens. Actuators B* 113:389–97

Rezk AR, Manor O, Friend JR, Yeo LY. 2012a. Unique fingering instabilities and soliton-like wave propagation in thin acoustowetting films. *Nat. Commun.* 3:1167

Rezk AR, Qi A, Friend JR, Li WH, Yeo LY. 2012b. Uniform mixing in paper-based microfluidic systems using surface acoustic waves. *Lab Chip* 12:773–79

Rogers P, Friend JR, Yeo LY. 2010. Exploitation of surface acoustic waves to drive microparticle separation and concentration within a droplet. *Lab Chip* 10:2979–85

Sankaranarayanan SK, Cular S, Bhethanabotla VR, Joseph B. 2008. Flow induced by acoustic streaming on surface-acoustic-wave devices and its application in biofouling removal: a computational study and comparisons to experiment. *Phys. Rev. E* 77:066308

Sankaranarayanan SKRS, Singh R, Bhethanabotla VR. 2010. Acoustic streaming induced elimination of non-specifically bound proteins from a surface acoustic wave biosensor: mechanism prediction using fluid-structure interaction models. *J. Appl. Phys.* 108:104507

Schlichting H. 1932. Berechnung ebener periodischer Grenzschichtströmungen. *Z. Phys.* 33:327–35

Schmid L, Wixforth A, Weitz DA, Franke T. 2012. Novel surface acoustic wave (SAW)-driven closed PDMS flow chamber. *Microfluid. Nanofluid.* 12:229–35

Schneider M, Guttenberg Z, Schneider S, Sritharan K, Myles V, et al. 2008a. An acoustically driven microliter flow chamber on a chip (μFCC) for cell-cell and cell-surface interaction studies. *ChemPhysChem* 9:641–45

Schneider S, Nuschele S, Wixforth A, Gorzelanny C, Alexander-Katz A, et al. 2008b. Shear-induced unfolding triggers adhesion of von Willebrand factor fibers. *Proc. Natl. Acad. Sci. USA* 104:7899–903

Seemann KM, Ebbecke J, Wixforth A. 2006. Alignment of carbon nanotubes on pre-structured silicon by surface acoustic waves. *Nanotechnology* 17:4529–32

Shi J, Ahmed D, Mao X, Lin S, Lawit A, Huang T. 2009a. Acoustic tweezers: patterning cells and microparticles using standing surface acoustic waves (SSAW). *Lab Chip* 9:2890–95

Shi J, Huang H, Stratton Z, Huang Y, Huang T. 2009b. Continuous particle separation in a microfluidic channel via standing surface acoustic waves (SSAW). *Lab Chip* 9:3354–59

Shi J, Mao X, Ahmed D, Colletti A, Huang T. 2008. Focusing microparticles in a microfluidic channel with standing surface acoustic waves (SSAW). *Lab Chip* 8:221–23

Shi J, Yazdi S, Lin SCS, Ding X, Chiang IK, et al. 2011. Three-dimensional continuous particle focusing in a microfluidic channel via standing surface acoustic waves (SSAW). *Lab Chip* 11:2319–24

Shilton RJ, Glass NR, Chan P, Yeo LY, Friend JR. 2011a. Rotational microfluidic motor for on-chip micro-centrifugation. *Appl. Phys. Lett.* 98:254103

Shilton RJ, Langelier SM, Friend JR, Yeo LY. 2012. Surface acoustic wave solid-state rotational micromotor. *Appl. Phys. Lett.* 100:033503

Shilton RJ, Tan MK, Yeo LY, Friend JR. 2008. Particle concentration and mixing in microdrops driven by focused surface acoustic waves. *J. Appl. Phys.* 104:014910

Shilton RJ, Yeo LY, Friend JR. 2011b. Quantification of surface acoustic wave induced chaotic mixing-flows in microfluidic wells. *Sens. Actuators B* 160:1565–72

Shiokawa S, Matsui Y, Ueda T. 1990. Study on SAW streaming and its application to fluid devices. *Jpn. J. Appl. Phys.* 29:137–39

Smorodin T, Beierlein U, Ebbecke J, Wixforth A. 2005. Surface-acoustic-wave-enhanced alignment of thiolated carbon nanotubes on gold electrodes. *Small* 1:1188–90

Tan M, Friend JR, Yeo LY. 2007a. Direct visualization of surface acoustic waves along substrates using smoke particles. *Appl. Phys. Lett.* 91:224101

Tan M, Friend JR, Yeo LY. 2007b. Microparticle collection and concentration via a miniature surface acoustic wave device. *Lab Chip* 7:618–25

Tan M, Yeo LY, Friend JR. 2009a. Rapid fluid flow and mixing induced in microchannels using surface acoustic waves. *Eur. Phys. Lett.* 87:47003

Tan MK, Friend JR, Matar OK, Yeo LY. 2010a. Capillary wave motion excited by high frequency surface acoustic waves. *Phys. Fluids* 22:112112

Tan MK, Friend JR, Yeo LY. 2009b. Interfacial jetting phenomena induced by focused surface vibrations. *Phys. Rev. Lett.* 103:024501

Tan MK, Tjeung R, Ervin H, Yeo LY, Friend JR. 2009c. Double aperture focusing transducer for controlling microparticle motions in trapezoidal microchannels with surface acoustic waves. *Appl. Phys. Lett.* 95:134101

Tan MK, Yeo LY, Friend JR. 2010b. Unique flow transitions and particle collection switching phenomena in a microchannel induced by surface acoustic waves. *Appl. Phys. Lett.* 97:234106

Tjeung RT, Hughes MS, Yeo LY, Friend JR. 2011. Surface acoustic wave micromotor with arbitrary axis rotational capability. *Appl. Phys. Lett.* 99:214101

Tran SBQ, Marmottant P, Thibault P. 2012. Fast acoustic tweezers for the two-dimensional manipulation of individual particles in microfluidic channels. *Appl. Phys. Lett.* 101:114103

Travagliati M, Simoni GD, Lazzarini CM, Piazza V, Beltram F, Cecchini M. 2012. Interaction-free, automatic, on-chip fluid routing by surface acoustic waves. *Lab Chip* 12:2621–24

Tseng WK, Lin JL, Sung WC, Chen SH, Lee GB. 2006. Active micro-mixers using surface acoustic waves on Y-cut 128° $LiNbO_3$. *J. Micromech. Microeng.* 16:539–48

White R, Voltmer F. 1965. Direct piezoelectric coupling to surface elastic waves. *Appl. Phys. Lett.* 7:314–16

Wijshoff H. 2010. The dynamics of the piezo inkjet printhead operation. *Phys. Rep.* 491:77–177

Wilson R, Reboud J, Bourquin Y, Neale SL, Zhang Y, Cooper JM. 2011. Phononic crystal structures for acoustically driven microfluidic manipulations. *Lab Chip* 11:323–28

Wixforth A, Strobl C, Gauer C, Toegl A, Scriba J, von Guttenberg Z. 2004. Acoustic manipulation of small droplets. *Anal. Bioanal. Chem.* 379:982–91

Wood CD, Evans S, Cunningham JE, O'Rorke R, Wälti C, Davies A. 2008. Alignment of particles in microfluidic systems using standing surface acoustic waves. *Appl. Phys. Lett.* 92:044104

Wood CD, Cunningham JE, O'Rorke R, Wälti C, Linfield EH, et al. 2009. Formation and manipulation of two-dimensional arrays of micron-scale particles in microfluidic systems by surface acoustic waves. *Appl. Phys. Lett.* 94:054101

Wu TT, Chang IH. 2005. Actuating and detecting of microdroplet using slanted finger interdigital transducers. *J. Appl. Phys.* 98:024903

Yeo LY, Chang H, Chan PPY, Friend JR. 2010a. Microfluidic devices for bioapplications. *Small* 7:12–48

Yeo LY, Friend JR. 2009. Ultrafast microfluidics using surface acoustic waves. *Biomicrofluidics* 3:012002

Yeo LY, Friend JR, McIntosh MP, Meeusen EN, Morton DA. 2010b. Ultrasonic nebulization platforms for pulmonary drug delivery. *Expert Opin. Drug Deliv.* 7:663–79

Yoon SH, Huang Y, Edgar JS, Ting YS, Heron SR, et al. 2012. Surface acoustic wave nebulization facilitating lipid mass spectrometric analysis. *Anal. Chem.* 84:6530–37

Annual Review of
Fluid Mechanics

Volume 46, 2014

Contents

Indexes

Errata

An online log of corrections to *Annual Review of Fluid Mechanics* articles may be found at http://fluid.annualreviews.org/errata.shtml